processes

MDPI

Review

A General Review of the Current Development of Mechanically Agitated Vessels

Marek Jaszczur [1,*] and Anna Młynarczykowska [2]

[1] Faculty of Energy and Fuels, AGH University of Science and Technology, 30-059 Kraków, Poland
[2] Faculty Mining and Geoengineering, AGH University of Science and Technology, 30-059 Kraków, Poland; mindziu@agh.edu.pl
* Correspondence: jaszczur@agh.edu.pl

Received: 7 July 2020; Accepted: 5 August 2020; Published: 13 August 2020

Abstract: The mixing process in a mechanically agitated vessel is a widespread phenomenon which plays an important role among industrial processes. In that process, one of the crucial parameters, the mixing efficiency, depends on a large number of geometrical factors, as well as process parameters and complex interactions between the phases which are still not well understood. In the last decade, large progress has been made in optimisation, construction and numerical and experimental analysis of mechanically agitated vessels. In this review, the current state in this field has been presented. It shows that advanced computational fluid dynamic techniques for multiphase flow analysis with reactions and modern experimental techniques can be used with success to analyse in detail mixing features in liquid-liquid, gas-liquid, solid-liquid and in more than two-phase flows. The objective is to show the most important research recently carried out.

Keywords: agitated vessel; stirred tank; fluid mixing; rotary mixer

1. Introduction

The mixing processes in an agitated vessel are widely used for various purposes and play an important role among industrial application. Fluids, as well as solids, mixing often comprises several phases and its primary task is as follows:

- to disperse one immiscible liquid into another or to combine miscible liquids; to disperse solid materials in a fluid, often followed by a different process, e.g., chemical reaction, leaching or flotation; to disperse gas into a liquid, usually followed either by a chemical reaction between the liquid and the gaseous species or by absorption; to disperse a solid and gas into a liquid phase to cause reactions.

For each application, various configurations and methodologies of the study are appropriate. In various processes, the overall efficiency and the final product quality depends on not only the physicochemical properties of all phases in mixing system, but also on the level of energy dissipation, and the impeller-tank configuration, in particular, on the detailed geometrical shape of impellers [1].

Therefore, mixing processes optimisation, as one of the most energy-consumptive steps in many industrial processes, necessitates the reassessment of the existing knowledge and often lead to even the development of the high-performance system, as well as an experimental method [2].

The suitability of the mixing system for a particular application can be evaluated by the specific qualification of the flow phenomena and flow pattern in a tank, as a complex function of:

- the internal vessel geometry or configuration (baffles, coils, vessel bottom type, etc. [3–6]);
- the fluid properties (densities, number of phases, a viscosity [7]);

- the location and mode of operation of the impeller (flow-pumping direction, clearance).

The continuous-flow mixing operations in mechanically agitated vessels are going to play an essential role in industrial processes. Continuous mixing mat significantly speed-up mixing mixture production; however, it is still challenging to maintain final product constant properties. In [8] authors analyse the volumetric mass transfer coefficient, considered as a critical transport characteristic in the design of mechanically agitated contactors. Based on their previous work, the correlation for mass transfer coefficient prediction in the coalescent batch were presented for Rushton turbines 8]. In a recent work, the authors evaluate single universal correlation that would be viable for mechanically agitated contactors in coalescent batch for any new impeller types with different diameters and their mutual position on a common shaft. Researchers have shown the correlation which can be used to predict transport characteristics in industrial-scale vessels for a wide range of operational conditions in the technological process.

The first analysis for the multiphase flow was performed using phenomenological methods, merely watching the fluid and eventually using some seeding like fluorescent or coloured material, or in more complicated situations, radioactive isotopes [9–11]. Later, the researchers used a simple measuring technique to quantify the velocity vector field [12], through laser Doppler Anemometry (LDA) [13], Laser-Induced Fluorescence (LIF) [14], Particle Image Velocimetry (PIV) [15–18], tomography methods in the standard [19,20] or advanced configuration [21].

Finally, to combining the computational fluid dynamic (CFD) and experimental method, treated as calibrated input data for numerical models and source for newly created models [22], e.g., in the mixing of glycerol and ethanol [23], the homogenisation of two mutually dissolvable fluids with very different properties [24,25], the water and ethanol system [26] and the blending of two or more miscible liquids with very different density and a viscosity [27].

The first analyses showed that the flow generated by the impeller is influenced by a large number of various factors, including the number of impellers [28], the size, shape and impeller type [29,30], the location and layout of the impeller [31] and rotational speed (see Figure 1).

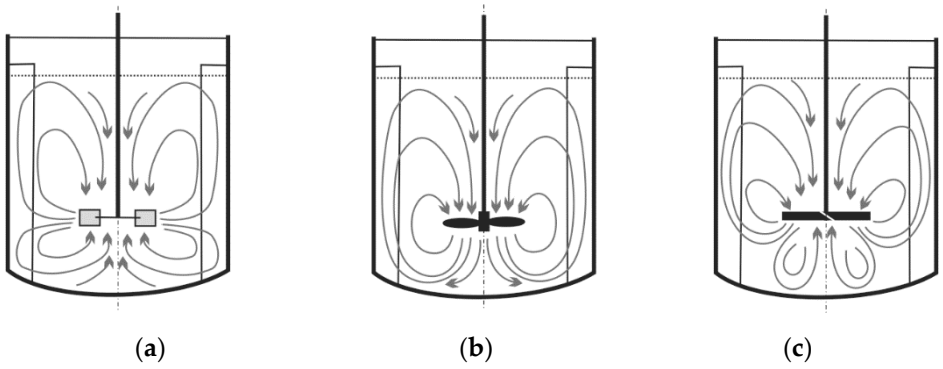

Figure 1. Flow motion generated by different impellers types: (**a**) radial; (**b**) axial; (**c**) mixed.

2. Mixing

2.1. Fluid Flow

In order to model the fluid flow, several assumptions have to be applied, including the assumption that, the hydrodynamics and fluid rheology are homogeneous in turbulent flow and referred the "perfectly mixed fluid" as the reference value in the mixing process. However, in real industrial processes, such cases do not occur, so neither the fluid regime nor the hydrodynamics timescales are known with certainty.

Non-Newtonian fluids with complex rheology are present in important industry sectors, such as biotechnology, chemical and wastewater treatment. Fernandes del Pozo et al. [32] analyse the

hydrodynamics of non-Newtonian flows at broad range Reynolds number generated by an axial impeller (A310) in a single-phase Carbopol fluid using CFD modelling and PIV measurement to validate results. The authors demonstrate that the flow field below the impeller is highly dependent on the rheological behaviour of the fluid. Similar impact assessment studies of hydrodynamic conditions on mixing process were presented by Abdulrasaq and Ayranci [33] and by Tsabet and Fradete [34], concerning the stability of Pickering emulsion (oil-water mixture with hydrophilic glass beads) in the baffled tank with Rushton turbine (RT) or pitched blade turbine (PBT). The authors found that the energy dissipated and the size of the high shear zone around the impeller are key information to create the emulsion with the desired droplet sizes.

Ali Sk et al. [35] reported that the heat transfer data for agitated Newtonian and non-Newtonian fluids related to Nusselt number depends on impeller diameter in the agitated vessel. The authors, by using experimental data, correlated viscosity with of Reynold, Prandtl number and Nusselt Number, which were evaluated at the impeller tip.

In the literature, different research groups use various indexes to describe the effect of mixer geometry and mixture properties on degrees of homogeneity suspension. In Table 1, the most common indexes widely used in the literature are shown.

Table 1. Indexes used by various research groups to describe degrees of homogeneity suspension with impeller type, effect and experimental method.

Index	Effect	Impeller Type [1]	Experimental Method	Ref.
D, μ, C, d_p	Axial flow impellers are more favourable for solid suspensions Increasing solids loading delays the homogenization in a more pronounced way for axial impellers The cloud height and the particle distribution increase with a larger clearance	PBT, RT, CBT, HE-3, A310, InterMIGs	Gamma-ray densitometry	[36]
D, C	N_{js} decreases when D increases ($\propto D^{-2}$) $N_{js} = f(C/T)$ shows 3 zones for PBT: $C/T < 0.1$, constant; $0.1 < C/T < 0.35$, slight increase; $C/T > 0.35$, steep increase	PBT	Visual observation	[37]
D	For $D = T/3$ impellers, higher efficiency than $D = T/2$ in turbulent regime For $T/3$ impeller, higher energy efficiency The power model aptly predicts of N_{js} for impellers in the full range of C and up to C_v = 27 wt%	A310	Visual observation, CFD	[38,39]
	$D/T = 0.35$ is the optimal ratio- $D/T = 0.35$ is the optimal ratio	PBT, HE-3	Visual observation CFD	[40]
	D = T/3 disk turbine shows poor ability to suspend particles in 1 Pa·s fluid	Mixed flow, HE3 InterMIGs	Visual observation	[41,42]
μ, C	Flow patterns change due to the dampening of axial circulation (_ up to 1 Pa·s). N_{js} and the specific energy dissipation rate ε_{js} increase when _ increases For 1 Pa·s fluid, N_{js} is minimum at $C = T/4$, as particle accumulation and significant momentum loss are prevented	RT, PBT, HE3, A310, InterMIGs	Visual observation	[43,44]
d_p, μ	The plurality of conclusions reflects the complexity of the effect of d_p, The multiplication of particle interactions leads to poorer suspension	LightninA310, PBT,	Visual observation	[45,46]
d_p, μ	Larger d_p implies larger settling velocity and higher N_H Higher settling times facilitate the homogenization once the particles have been lifted	A100, A200, A310, A320	Electrical resistance tomography (ERT), CFD	[47,48]

Table 1. *Cont.*

Index	Effect	Impeller Type [1]	Experimental Method	Ref.
d_p, C_v, μ	Defined mixing index (*MI*) as a homogeneity measure *MI* improve with impeller speed increasing, approx. 0.8 N_{js} for increase particle size For the fine fraction, *MI* depends on the range 0.5 N_{js} to 1.4 N_{js}.	RT	ERT	[49]
D, d_p, μ, C	Smaller particles are easier to suspend in water N_{js} is independent of d_p for unbaffled tanks N_{js} decreases when _increases for baffled tanks The most efficiency of aerobic bioremediation of soils is to an unbaffled bioslurry reactor stirred by a Rushton turbine with $D = T/3$ and $C = T/3$	RT, A310	Steady cone radius method, Laser Sheet Image Analysis (LSIA)	[50–53]
	Axial impellers exhibit a radial profile that leads to a less efficient suspension taking place at the centre	RT, PBT, A320	Visualization techniques	[54]
	Due to a decrease of the settling velocity, higher _ results in smaller N_{js}	A310, PBT, DT	Laser Doppler velocimetry	[55]
	Mixing times are larger for large solids concentrations (>10 wt%)	PBT, DT, propeller	Decolorization method	[56]
	Above 10 wt% of solids loading, the blend time increases, and there is a clear layer at the surface	A-310, A-315, InterMIGs	Decolorization method, visual method	[57]
C, C_v, D	N_{JS} (expressed as $N_{Fr,JS}$) and $(P/m)_{JS}$, and one can note that an increase in solid concentration *(Cv)* has an influence on N_{JS} values $N_{Fr,JS} \propto C = 0.13$ (visual method) $N_{Fr,JS} \propto C = 0.12$ (conductivity method) the values of N_{tm}, and N_{JS} decrease with an increase of impeller diameter N_{tm} is the lowest for $(D/T = 0.45)$	PTD-two down-pumping	Joosten visual method, conductivity method	[58]
D, d_p, C, C_v	The use vessel with baffles enhanced the H_o obtained by the Maxblend impeller for optimal rotor speed and fixed particles content (N = 180–600 rpm; d_p = 209–752 µm; C_v = 5–30 wt%; C = T/8–T/4 The extent of homogeneity and mixing index in the system increase with the agitation speed The highest H_o for the impeller clearance of C = T/8.	A200, RT, Maxblend	ERT	[59]
D, d_p, C, X	Increasing the particle size resulted in an increase in the just-suspended speed and power number (A310) The extent of homogeneity was enhanced with the decreasing particle size from d_p = 5000 to 753 µm The highest homogeneity (H_o) by reducing the solids loading from X = 55.0 wt% to 30 wt%.	PBT, PF3,A310	ERT, CFD	[60,61]
μ, D,	The mixing time of coaxial mixer increased when the consistency index and yield stress were raised	DSAC; SSAC,	ERT, CFD, statistic	[62,63]
μ, D, T	The power consumption and mixing time were determined for used impellers system	DSAC, DPBTAC		[64]

Table 1. *Cont.*

Index	Effect	Impeller Type [1]	Experimental Method	Ref.
	The mixing of the viscous non-Newtonian fluids			
μ, D	The coaxial mixers are more efficient for the mixing of yield-pseudoplastic fluids Multi-impeller mixers are more compact for the larger scale of mixing operations The coaxial mixer system composed of double Scaba impellers and an anchor was the most efficiency	DSAC, Scaba-Rushton-anchor, Scaba- anchor, Scaba-PBT PBT–Scaba	ERT, CFD	[65]
μ, d_p, C_v, d_b	The air superficial velocity causes the increase gas hold-up to 19% for the column operating with growing solids concentration (5–15%) The gas hold-up decreases with the solids content.	No rotor-air mixing	ERT, pressure transducers (PT)	[66]
X	The decrease inhomogeneity index for increasing X down to a plateau, and finally a small increase inhomogeneity at large X.	4PBT	positron emission (PEPT), CFD	[67]
d_p, μ, X_v, D, C	The increase in D leading to a decrease in N_{js} N_H, The homogenization with large impellers is easier Higher clearances is hindered for large particles	two PBT	pressure gauge technique, ERT	[68]
d_p, C_v, T	The increase of C_v significantly increases the mass transfer coefficient due to increase N_{js} The mass transfer coefficient as a measure of the effectiveness of the suspension	RT	Visual method	[69]
d_p, C_v, X, ϱ_s, ϱ_l, μ, T	Re_E and N_{JS} are proportional to $(T/D)^{1.50}$ and independent of (C/T), The high shear is beneficial with using very high C_v.	RT	Visual method	[70]
D, C, X, μ, C_v	The larger impellers (up to a max D/T = 0.5) outperformed smaller ones The baffles inhibit the suspension of powder with the C_v increases As the C_v increases, the flow regime changes, from laminar to turbulent	RDT6, UP-PBT4, DP-PBT4, A310 hydrofoil, Torrance sawtooth	Visual method	[71]
d_p, d_b, μ, C_v	The k_La decrease with a fall in gas hold-up In the salt, solution k_La decreased to 40% for C_v = 0 wt% and around 19% solids by volume of dispersion	6HBT, 6MFU-45°	Visual method	[72]
d_p, μ, C_v, w	$(C_v)_{max} = C_{vb}$ = 0:90, with baffles $(C_v)_{max} = C_{vb}$ = 0:98, without baffles: the average optimum C_v with min. power consumption, is the range 0.25–0.35 v/v the ε_{js} values decrease with an increase the number blades of impellers each impellers type can be a critical particle size	DT6, DT4, DT3, 30PBT6, 20-45PBT4, 30PBT3, A310	Visual method	[73]

[1] PBT: pitched blade turbine, FBT: flat blade turbine, DT: disk turbine, RT: Rushton turbine, RDT6-CBT: curved blade turbine, HE3: high efficiency impeller, A100: Lightning propeller, A200: Lightning PBT, A310: Lightning low viscosity impeller, A320: Lightning low Re impeller., ASI: single axial-radial flow impeller, DSAC: dual Scraba coaxial impeller, SSAC: single Scaba-anchor coaxial, DRTAC-dual Rushton turbines system with an anchor impeller of coaxial; DPBTAC dual pitched blade turbines with an anchor impeller of coaxial; UP-PBT4: up-pumping pitched blade impellers, DP: PBT4-down-pumping pitched blade impellers, 6HBT: parabolic blade, 30PBT6-30° pitch 6-bladed turbine, 20PBT4: 20° pitch 4-bladed turbine, 30PBT4: 30° pitch 4-bladed turbine, 45PBT4: 45° pitch 4-bladed turbine, 30PBT3: 30° pitch 3-bladed turbine.

2.2. Gas-Liquid and Gas-Liquid-Liquid System

In [19], results obtained from an innovative approach which describe the behaviour of gas-liquid mixing, i.e., electrical resistance tomography (ERT) were shown. The authors further used the dynamic gassing-out method in the tank with baffles during the input power measurement in order to find mass transfer coefficient k. They used selected working parameters to test the proposed methodology

by changing the number of baffles in the ERT system. Based on experimental results, it was shown that the optimum numbers of baffles, which reduced the energy input cost by as much as 54%, is four.

Three-phases, the gas-liquid-liquid system configuration, may occur in many industrial processes with the chemical reactions. This often includes multiphase systems which enable the effective recycling of homogeneous catalysts and costly organometallic complexes [1]. Results presented in the paper by Schrimpf et al., confirm that the presence of additional phase positively impacts the mass transfer coefficient, but the authors do not explain the exact mechanism by which this improvement is obtained. In gas-liquid systems generated in a vessel with one or more impellers, the primary target is to obtain uniform gas dispersion throughout the whole volume of the liquid. As show literature studies, the dispersion depends on the type, size and location of gas sparger [74,75].

The energy consumption by the impeller is one of the crucial parameters for assessing the effectiveness of mixing under the influence operating parameters of a process and physical parameters of a fluid, as well as the amount of gas supplied to the system [76,77]. In the research presented by Cudak [78] the focus is on hydrodynamic characteristics of aqueous at low concentration sucrose mixture by using the Rushton turbine, the Smith turbine and the impeller A-315 type. Based on the results, optimal mixing conditions were evaluated. The Rushton turbine was not recommended to biological processes with microorganisms and processes which are very sensitive to the shear stress. At another research work by Cudak et al. [79] a comparative analysis based on experimental data concerning the impact of the impeller geometry and baffles geometry, number and shape of impellers, the scale of the agitated tank, as well as their off-bottom clearance and properties of the multiphase systems on the critical impeller speeds, were investigated. The authors conclude that in order to generate dispersion or suspension, energy consumption and gas hold-up have to be considered in parallel in order to enable appropriate conditions to drawdown or suspended particles, as well as to disperse small and large air bubbles in liquids. The most reliable criterion to evaluate the state of a multiphase system is the agitation energy requirement expressed as agitator power per unit solids mass at the just-off-bottom solid suspension condition (ε_{js}) or as ratio power to tank volume (P/V). In addition, it should be noted that any changes to any factor described the agitator could significantly impact the behaviour of an agitated gassed suspension. The absence of coalescence in a rotating gas-liquid or gas-solid- liquid system results in the highest gas hold-up (φ).

2.3. Electrical Resistance Tomography (ERT) in Gas—Liquid System

The hydrodynamic performance of the ASI impeller in an aerated bioreactor containing the biopolymer solution through tomography and CFD modelling was assessed by Khalili et al. [80] based on analogical measurement system (mixer and non-Newtonian liquid) and methodology. The new impeller (ASI) dedicated to the gas dispersion in highly viscous fluids compared to Rushton turbine (with and without pitched blade) demonstrated the minimal impact of the gassing (measured as gas holdup) on power consumption (36%) versus the Rushton turbine (50%). They were thus proving the high energy efficiency of the ASI impeller.

Gas-phase characteristics were analysed as well by Babaei et al. [81,82] as an important hydrodynamic parameter influence to the oxygen distribution in activated sludge. The authors used the dynamic gas disengagement (DGD) and ERT technique to determine gas phase properties including: bubble size, bubble rise velocity, the quantity of bubble size classes, the contribution of each class to global gas holdup and specific interfacial area of mass oxygen transfer in an activated sludge bubble column bioreactor under set conditions of the process. Based on the results, a correlation was presented between bubble size to the aeration rate and sludge rheology. The complexity of the analysed process made it impossible to formulate unambiguous conclusions.

A similar methodology was used in [83]. They analysed the hydrodynamics of gas-liquid two-phase flow in a bioreactor using the ERT and dynamic gas disengagement (DGD) and CFD. Based on the modelling technique and experimental methods, they were assessing the impact of the volumetric gas flow rate and rotor speed on the gas-liquid flow field, the gas holdup values and Sauter

mean bubble diameter. The results have shown that the global gas holdup values increased with increasing both the impeller speed and volumetric gas flow rate. The CFD model indicates that a more uniform dispersive of the gas holdup was obtained at impeller speeds ≥100 rpm for volumetric gas flow rates $\geq 1.6 \times 10^{-5}$ m^3/s.

A very important issue to enhance the efficiency of the aerated mixing vessel is the designation of the flow pattern hydrodynamics by the impeller, which influences the bubble size and gas holdup [84]. The main characteristics of the gas phase were measured by using the dynamic gas disengagement theory with combined ERT data. The results have shown that the bubbles generated at the central plane of the impeller plane were smaller than those generated at the bottom the impeller. The local and global gas holdup values and the Sauter mean bubble diameter was estimated. A working liquid was used, the viscous corn syrup solution, which had been mixed by aerated coaxial mixing vessel with impellers coaxial system (PBT and Anchor rotor). This demonstrated that the bubbles break up under the influence ratio speed of anchor blades and the minimum global of gas holdup obtain at the speed ratio of 10 for independently from gas velocities. In another paper [85], the authors developed characteristics of aerated corn syrup solutions as a Newtonian fluid in a reactor with coaxial mixer system, such as: the anchor—PBD (a pitched blade downward pumping impeller) and the anchor—PBU (a pitched blade upward pumping impeller). As a measurement technique was used electrical resistance tomography (ERT). Analysed the effect of aeration on the mixing time with different of hydrodynamic regimes occurring in the vessel. The experiments have shown that the mixing time is a function of parameters responsible for the hydrodynamics conditions. It was indicated that the response surfaces method could be used to visualization the mixing processes of the higher viscosity liquid. The tally of literature, after the year 2000, about gas holdup determination by different technique measurement with short characterisation and various gas holdup correlations can be used to analyse experimental data, as was reported by Sardeshpande et al. [86].

During the mixing process, the non-Newtonian liquids often repeat zones around the rotor zones of intense liquid motion surrounded by stagnant zones in the mixing vessel.

In [87], the authors use electrical resistance tomography and computational fluid dynamics modelling to study the formation of a cavern in the mixing of pseudoplastic fluids possessing yield stress and drew attention to the phenomenon of caverns (zones of intense liquid motion) generated around an impeller. The sizes of caverns were analysed using ERT and modelling by Elson's model (cylindrical model) and obtaining good agreement between both approaches in the laminar and transient regime up to Re = 200. The experimental equipment contained a 4-plane 16-sensor ring ERT system ERT and a radial-flow Scaba 6SRGT impeller in a central position of the tank. A working liquid was used: a xanthan gum solution (pseudoplastic fluid possessing yield stress). This was based on the CFD model prepared characteristic of flow pattern description by pumping capacity, flow number, power consumption.

2.4. A Solid-Liquid System in a Mechanically Agitated Vessel

Wanga et al. [73] show analysis of energy required to suspend water–solid slurries in a rotating vessel over a wide range of geometries and boundary conditions. The research objective was to increase the mixing performance. The authors showed that the energy required to provide off-bottom solids suspension and dispersion could be significantly decreased with baffles removed, in reference to the conventional agitator designs where a vessel with baffles was used. The impellers, which generate the axial flow in a vessel with baffles, were found to have a higher performance to suspend solids off the tank bottom. For the mixing tank without baffles, radial-flow impellers were found performed better than axial flow impellers. The impeller shape analysis includes the number of blades and the pitch angle of the blade on an energetic performance. The impacts of particle concentration and particle size on energy consumption were also analysed [52].

Most of the studies carried out in the literature took into low account solids concentration systems [88] and were tested in vessels with impellers (either radial or axial). Only a limited number

of studies concentrate on analysis with the high solid concentration up to 50% (by weight). However, it should be noted that very highest solid contents (above 40%), reveal the central vortex which causes that solids are no longer brought directly to the impeller, and at the same time, instead of clumps, semi wetted powder agglomerates. Wood et al. [71] investigated the effect of high solid content on the drawdown and floating of solids in a mechanically agitated vessel. The authors analysed the effect of vessel configurations (impeller size and type) on concentrated alumina slurries in stirred tanks. The pitched blade impellers were found to be the most effective across various configurations. It was found that at high solids content (above 50% by weight) the demand for energy increasing dramatically, a nearly 100-fold.

Jafari et al. [36] showed detailed particle concentration distribution in dense solid–liquid suspension, investigated at laboratory scale. The authors specified scale-up rules to achieve the same level of homogeneity in a large vessel. The evaluated uncertainty of the sedimentation–dispersion models confirmed its capability to describe complex phenomena in dense liquid-solid mixing systems.

The vessels with single [89] mechanical agitator or multiple agitators systems are often used in various configurations in three-phase or two-phase mixing processes [90], such as catalysed oxidation, polymerisation, evaporative crystallization [91], aerobic fermentation, [92] froth flotation [93], flocculation [94], microbial coal desulphurisation, gold leaching, bacterial, sulphide oxidations or separation processes etc. In all these applications, simultaneous dispersion of gas and the suspension of the solids have crucial meaning. In the systems carrying out the chemical reactions and physical mass transfer processes, two or three-phases are usually in contact, i.e., gas-liquid-solid, in which, the liquid is the continuous phase, while the solid or gas phase is considered as a discrete phase. In mixers with aeration system usually used in industrial processes, the solid particles are suspended entirely over the whole domain to expose their total surface area for the reaction or mass transfer. This kind of agitator operation provides to liquid mixing an active contact between the phases to establish hydrodynamic conditions for a single or multiple impellers system.

Kasat et al. [95] shown an interesting review on experimental works on solids suspension in mechanically agitated tanks. The authors reviewed various techniques used for the measurement of the selected quantitative and qualitative parameters of mixing processes for specified experimental conditions. The presented research review critically surveys the literature and makes recommendations for the use of appropriate conditions for experimental set-up as well as correlations in order to obtain reliable data. Some issues have been well described and remain valid today. The authors indicate that the critical parameters for the assessment of the efficiency of the impeller for solid suspension both in the presence of gas (N_{jsg}) and in the absence (N_{js}), are the impeller rotational velocity, which guarantees complete detachment of the solid particles from the vessel bottom and proper homogenisation. Based on a critical analysis of literature from before 2005, authors came to the main conclusion that: as the research studies show, N_{jsg} is always higher than N_{js} and for a given three-phase system N_{jsg}, depends on the design parameters of the rotor, sparger and their mutual relationship. Therefore, by selecting a proper configuration of the above parameters, the gas dispersion characteristics and solid suspension of the agitator can be significantly improved and made a thereby large reduction in required power. The authors recommended the measurement of local values for solid concentration using the only non-intrusive optical technique to determine the minimum value N_{js} and N_{jsg} in transparent vessels. The experimental measurement of power consumption and mixing time for large and opaque vessels and at the same time, require to develop the pressure measurement techniques. It was found that the overall values for solids concentration in the vessel is important, and not the local value, as the best configuration for simultaneous gas dispersion and solid suspension. The recommendation is to the impeller with a reversible mode and located at an off-bottom clearance of C = T/4, and using a ring sparger with ring size larger than the impeller diameter (d_s = 1.5D–2D) and installed below the rotating impeller or in the stream which output of the impeller.

In other research studies, Abdel-Aziz [96] describe the rates of solid-liquid mass transfer in correlation to diffusion-controlled corrosion at the outer surface of helical coils immersed in unbaffled

agitated vessels. It was shown that for axial and radial flow impellers the solid-liquid mass transfer is higher than for axial flow type, and the difference is in the range of 16–41%, depends on operating conditions. A similar mass transport system which occurs in electropolishing processes was discussed by Sedahmed et al. [97]. This process typically is used to metallographic examination in order to identify the microstructure of metals and to remove deformed surface zone produced, as an inspection tool reveal any microstructural defects (e.g., for nuclear equipment, high-pressure vessels and turbine blades for jet engines) and to provide a smooth, clean surface (for food, chemical, pharmaceutical and polymer industries). The authors realised experiment in a rectangular cell stirred by four blades 45' pitched turbine and indicate the optimal hydrodynamic and process conditions suitable to increase the efficiency of the electropolishing processes.

In chemical, food and biochemical industries, the mechanically agitated gas-liquid reactors are used, which requires specific geometry as well as agitator operating conditions [97]. Therefore, empirical modelling of mixing systems is quite common. The key parameter for bioprocesses is the volumetric mass transfer coefficient (k_La) during which the gas-liquid mass transfer rate is controlled. Petrícek et al. [98–101] examined typical situation for aerobic fermentation (the biomass is shear-rate sensitive) in which viscous batches are usually used, in term of impeller shape and vessel size using Rushton turbines in single- double- and triple-impeller configurations. Based on the experimental data and by using the dynamic pressure method (DPM), the authors applied two different approaches. In the first one, they determined the specific total power input with gas expansion (input-PTOT), and in the second one, they relied on impeller tip speed (ND) analysis. The authors were developed correlations to predict k_La value in industrial fermenters. Finally, the evaluated results showed similar standard correlations.

In another work, Perticik et al. [102] performed measurements for three-phase multiple-impeller fermenters with microparticles of diameter 137 ± 30 micrometres and presented the results in the form of mathematical relationships, between k_La and impeller power input, superficial gas velocity and impeller blade speed. The developed methodology can be widely used in industrial type vessels for cases where solid particles affect the interfacial mass transfer. In [103], the authors improved scaling-up methodology based on k_La related to the impeller power number and tip speed is proposed. However, the results indicated dependency between process conditions using various impeller types and k_La value. Dimensional analysis and CFD simulations of microcarrier 'just-suspended' state in mesenchymal stromal cells bioreactors were studied by Loubière et al. [104], using the Zwietering's model. The authors found that in the case of microcarrier suspension the number of particles is better optimisation parameter than the ratio diameter of particle per diameter of the impeller ($d_p = D$), while determining the model impeller constant (K), allows to classify impellers by calculation the up-pumping to lower N_{js} values.

2.5. Solid Suspension

In the research studies of Kraume [56] and Bujlaski et al. [57], the authors analysed the states of particle suspension occurring in the solid-liquid rotating vessel in reference to the rotational speed (Figure 2) and drew the following conclusions for low angular velocity, all the solids particle were deposited at the bottom of the tank Figure 2a, then with increasing angular velocity, the particles get lifted by the rotating flow and become suspended up to a certain distance from the bottom Figure 2b; further, increasing the impeller angular velocity causes all the solids to be lifted from the bottom of the vessel and remain in suspension for 1–2 s, thus obtaining complete off-bottom suspension.

The impeller speed corresponds to one defines as N_{js}. At this stage, a phase boundary appears between the clear liquid and the suspension Figure 2c; further, an increase in the impeller speed above of N_{js} value, generate the separation line to move up; and finally, when the slurry height amounts to 90% of the total liquid height Figure 2d, a suspension formed and the necessary condition defined by Bujalski et al. [57] and Drewer et al. [105] has been met; a further increase of impeller speed distributes

the solid particles and create the homogeneous distribution of solid particles throughout the vessel domain Figure 2e.

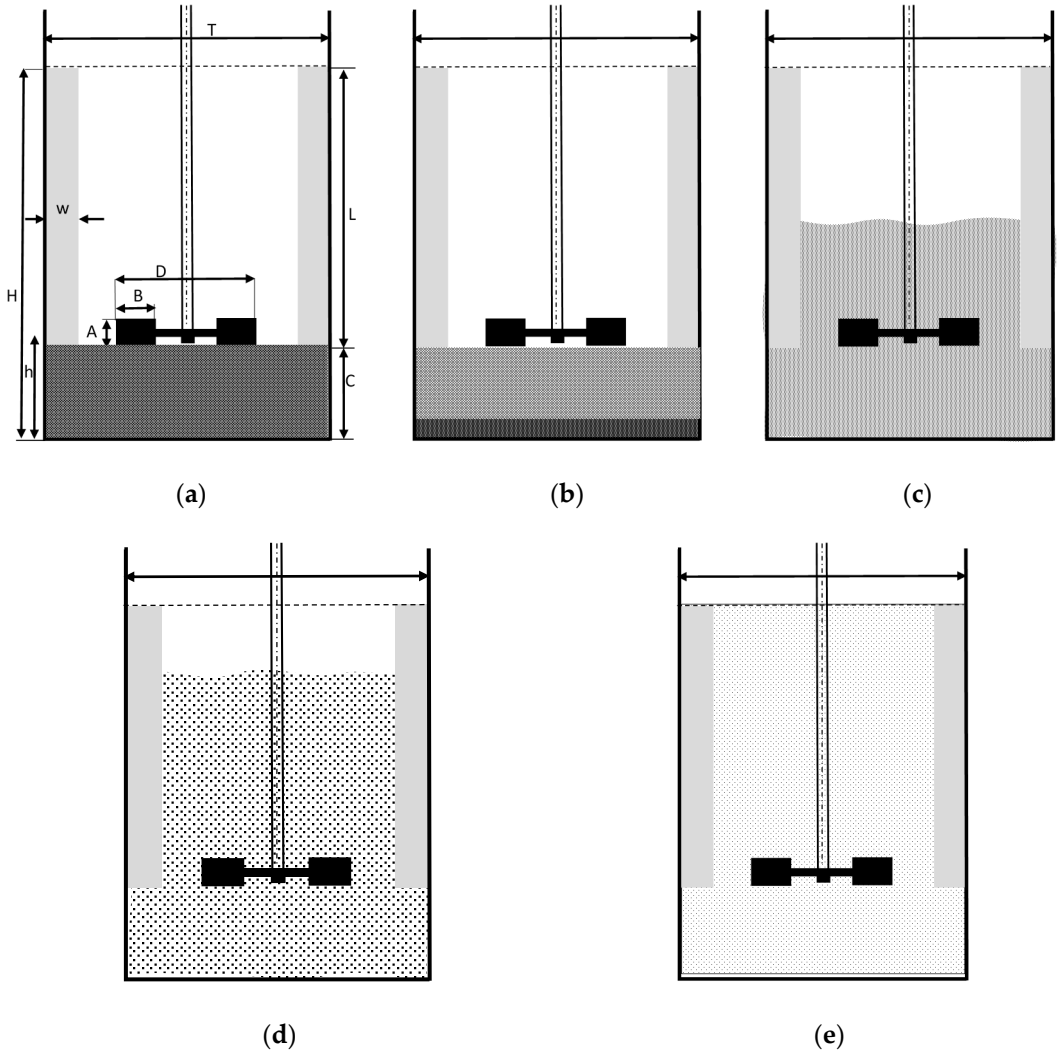

Figure 2. Particle suspension in the solid-liquid rotating vessel in reference to the rotational speed: (**a**) particle deposited at the bottom of the tank; (**b**) particles get lifted by the rotating flow; (**c**) clear liquid and the suspension line; (**d**) suspension the necessary condition; (**e**) homogeneous distribution.

Kasat et al. [106], reported that excessive energy is required to remove small amounts of solids from stagnant regions, notably near the baffles or at the centre of the vessel bottom. This is the case when the weaker fluid rotation at these locations occurs. To prevent stagnation, about 20–50% increase in angular velocity is required for off-bottom solids particle suspension [55,106–108]. To determine the value of N_{js}, the authors used an inverted experimental method, i.e., the impeller speed was increased to tear all of the solids from the tank bottom and create a homogenous slurry, and then the impeller speed was then decreased gradually until a thin layer of solid particles appeared at the vessel bottom. Under these conditions, the impeller rotational velocity was again significantly increased gradually to the designated as N_{js} value at which the solids bed disappeared.

To evaluate energy consumption during solids suspension in an agitated vessel the specific impeller consumption (ratio of agitator power required for just-off-bottom solids particle suspension to vessel volume-(P_{js}/V) can be used and specific impeller power requirement ε_{js} ($\varepsilon_{js} = P_{js}/M_s$, where M_s it's solids mass) at N_{js} are depend to solids concentration (C_v), particles size and impeller type [109]. The above parameters dramatically increase after exceeding the certain specified of minimum value

C_v for the same rotor. In addition, the presence of baffles increases power consumption and hinders dispersion of solids, just like increasing particle size regardless of vessels type with or without. It has also been shown that "axial-flow" impellers (HE-3, Chemineer P-4, A-315, A-310, MaxFlow-MX-4) in baffled tanks are more efficient to suspend solids off the bottom, but the radial-flow impellers (Rushton turbine, DT3, DT4, CD-6) are the most efficient but in vessels without baffles. Wang et al. [108] have been studied the impeller power required to get up the off-bottom suspension with very high solids concentrations (up to 55%) in an agitated vessel with baffles and without baffles. Authors indicated that the ratio of maximum available solids concentration at N_{js} to solids bed-packing coefficient $(C_v)_{max}/C_b$ is approx. 0.98 under unbaffled conditions, and approx. 0.90 under baffled conditions. The specific power input (P_{js}/V), defined as impeller power input at N_{js} per unit slurry volume was calculated to assess the effect of impeller type on suspension lifting efficiency. It has been shown that the disc turbine requires the lower specific power than the pitched bladed or hydrofoil impellers under baffled conditions. Under unbaffled conditions, this observation is different from reported in the literature [109–111] which showed that at higher power number mixing is more efficient under unbaffled conditions (C_v = 0.40 *v*/*v*, solids volume concentration). The best solid particles concentration at which ε_{js} is minimum and ratio P_{js}/M_s is evaluated as the total mass of solid particles suspended, also defined by Drewer et al. [105]. This parameter is independent of liquid viscosity but is dependent on the impeller type. Baffles removal is found to be beneficial to increase the intensity of the process. It results in about 80% energy consumption reduction by the impeller, even for very viscous fluids.

2.6. Solid Particle Distribution—Selected Technique

Basic measurement techniques for the solid particle distribution inside a stirred vessel can be classified into two groups: intrusive and non-intrusive techniques. For experimental analysis probe measurement (works well with high solid concentrations and are strongly sensitive to local flow conditions) [69,111–113], the optical method (based on light measurements) and acoustic techniques (measure the acoustic properties of a transmitted sound beam, such as sound speed and amplitude) in a continuous single-phase liquid systems are used. In such systems, other phases are dispersed (gas bubbles or solid particles), and these inhomogeneities are identified based on physics laws [112,113]. Practically, by quantifying this attenuation in acoustic technique, it is possible to calculate the relevant dispersed phase hold-up inside medium [69,114]. Optimum solids concentration for solids suspension and solid-liquid mass transfer in agitated vessels was reported by Bonga et al. [69], for low concentration of solids under various fluid viscosities. In a system, with the solid-liquid mixture, the accurate measurement of slurry viscosity is a severe task as the high solid particle concentration, as well as a concentration gradient, varies significantly throughout the vessel. It usually requires simplification, which is evenly distributed throughout the tank and determined apparent slurry viscosity using an empirical correlation proposed by many authors (for example, relationship according to Fedor). Authors estimate slurry viscosity as a function of solid concentration (C_v). From the experimental measurements, it has been recognised that the slurry remains comparatively constant with an increase in particle concentration to up specific value 0.20 (*v*/*v*), and then significantly increase. This situation can be explained by the strong interaction between particle-particle, thereby leading to a significant decrease in the mass transfer rate.

The experimental measurement of N_{js} and N_{jsg} with flow visual method in the stirred tank was presented by Mavros [12]. The presented techniques used in their study of the flow patterns induced for the various agitator's type i.e., classical pressure or velocity measurement with Pitot tubes or hot-wire anemometers, and novel ones like LDA, PIV and LIF are reviewed and their usefulness for particular situations is analysed. In order to determine the critical impeller rotation, speed for particle suspension in the presence of gas (N_{jsg}) should be suitable to the impeller geometry, the effect of off-bottoms and the effect of sparger design and its location, as well as the effect of solid properties and the effect of multiple impellers, to flow pattern.

The effect of impeller type was investigated by Abdel-Aziz [96], who reported results of the mass transfer in solid-liquid at the outer surface of helical coils immersed in the unbaffled agitated vessel by the diffusion-controlled dissolution of copper in oxidising environment solution. Various important parameters were investigated: impeller rotation speed, impeller geometry (four-blade turbine, pitched 90° axial flow type and 45°- radial flow type), coil pitched and physical properties of the solution. The authors showed that impeller rotation speed increase for axial flow type turbine results in increasing the solid-liquid mass transfer, while for radial flow type impeller, the mass transfer was found to increase with decreasing the coil pitch.

2.7. Electrical Resistance Tomography (ERT) in the Mixing of Highly Concentrated Slurries

One of the advanced and effective techniques widely used in the assessment of the gas-liquid, solid-liquid, liquid-liquid, and non-Newtonian fluids is the tomography technique, as well as the mixing operations is the mixing of highly concentrated slurries.

The hydrodynamic conditions inside the tank with a mechanical agitator are of fundamental importance. The agitators are usually classified as radial- or axial-flow impellers because they generate different flow patterns inside the tank. The type of flow patterns leads to different hydrodynamic behaviours during mixing and affect the efficiency of solid suspension create. Two forces work together on the particles to suspend them near the vessel: the drag force exerted by the moving fluid and the lift force created by bursting of turbulent eddies originating from the bulk flow inside the vessel. Thus, particle suspension in turbulent flow can result from a balance between the energy supplied by impeller rotation and energy required to lift solid particles. For this reason, choosing the right impeller, which can generate both the flow and turbulent intensity required for suspending solid particles in a highly concentrated slurry, is very important requires. These systems are used to many chemical engineering processes that deal with dense suspensions of large solid particles in the liquid.

In many works the machine with Electrical Resistance Tomography (ERT- a non-invasion and non-intrusive flow visualization technique) system was used to determine the degree of homogeneity within the slurry vessel [47–49,59–65,80–86,115]. Kazemzadeh et al. [60,116] used the electrical resistance tomography (ERT) to determine the degree of homogeneity and solid particle distribution inside the slurry reactor. They analysed qualitative and quantitative parameters to obtain information on the distribution of large solid particles and its effect on the mixing quality, for three axial impellers: PBT, A310 and PF3. Based on computational fluid dynamics simulations conducted using a Eulerian–Eulerian multiphase mode and experimental results, these indicate that the PBT impeller was the most efficient in terms of consuming power (greater homogeneity with the same power consumption), of generating velocity and turbulent kinetic energy within the mixing tank (the highest radial, axial and tangential velocities, below the impeller) and CFD and use of analogous measurement methods of ERT and computational fluid dynamics model was developed by employing the Eulerian-Eulerian multiphase model and the sliding mesh technique. The work [61] analysed the state of homogeneity in the slurry vessel with large particles in the highly concentrated. It was found that the energy loss was increase with the particle size changed from d_p = 753 μm to 5000 μm due to an increase in the collision between particles and interaction solid-liquid and solid-wall, inside reactor. Thus, with the decrease particle size is achieved the highest homogeneity and cloud height. Similarly, energy consumption increased when the solids loading increased from 30 to 55 wt% (weight). Therefore, the highest homogeneity was attained for a lower content of solids. It is shown that the suspension of large particles in slurries requires a higher turbulence intensity and a strong liquid circulation to compensate or overcome the gravitational and inertia forces on the solids particles with simultaneously reduced the impeller clearance.

In [63], the authors based on previously published correlations for the power consumption for a wide range of the rotation speed, for the coaxial mixers (a combination the Scaba and an anchor impeller) with pseudoplastic fluids (xanthan gum solution) as working fluids; the authors analysed the performance of DSAC (the double Scaba-anchor coaxial.) and SSAC (the single Scaba-anchor coaxial)

mixers in the mixing process. The CFD and ERT techniques were used to prepare flow profile and optimize working conditions for both, whereas the fluid rheology described by the Herschel–Bulkley rheological model. In [62], the authors analyse an impact of the rheological parameters (e.g., consistency index, power-law index and yield stress) by Herschel-Bulkley model (e.g., xanthan gum solution) on the mixing efficiency of a coaxial mixer (Scaba-anchor) at a different rotation speed, measuring the mixing time (ERT) and power consumption. The 3D simulation of CFD modelling (the sliding mesh method) showed that both the mixing time and power consumption increased with increasing the consistency index and yield stress, whereas they decreased with a rise in the power-law index. Model validation showed that the most important interaction between the consistency index and yield stress has occurred.

In a similar paper [64], based on the aforementioned techniques, authors analysed different coaxial mixers used to the biopolymer solutions (non-Newtonian liquids) mixing, like dual Scaba impellers system (DSAC), dual Rushton turbines system or dual pitched blade turbines with an anchor impeller. The results showed that the DSAC mixer was the best performing mixing system for the non-Newtonian fluids mixing of highly viscous because it created a more unitary velocity profile throughout the vessel compared to the others coaxial mixers system tested. Continuing the above research topic [65], they assessed multi-impeller coaxial mixers system. This system, composed of two different central impellers and an anchor, was dedicated to shear-thinning fluids possessing with yield stress. In this study the following systems were used: the Scaba-Scaba-anchor, Scaba-Rushton-anchor, Rushton-Scaba- anchor, Scaba-pitched blade-anchor and pitched blade-Scaba-anchor. These were analysed for their behaviour in a wide scope of Reynolds numbers. The results showed that multi-impeller coaxial mixers system is more compact and efficient for the mixing of yield-pseudoplastic fluids, indicating to Scaba-pitched blade-anchor coaxial system as having the most efficient in mixing. The correlation for a description of complex configurations of the coaxial mixers was introduced by the Metzner-Otto constants (Ks) for the different impellers types in the central position depending on the Reynolds number.

Hosseini et al. [47], presented the influence of elementary parameters, such as impeller type (Lightnin A100, A200, A310, and A320 impellers), impeller speed (250–800 rpm), impeller off-bottom clearance (T/5–T/2, where T is the tank diameter), particle size (210–1500 μm) and solid concentration (5–30 wt%) on the degree of homogeneity. The experimental data have shown that there is an optimal rotation speed which provides the maximum homogeneity (the A320 rotor was the most effective than the A200 impeller), whereas continuous increase the impeller speed will be detrimental; the increase of solids particles concentrate, changes the free settling velocity due to an increase in particle–particle interaction and contact with a stream of fluid flow upwards.

In [8], the mixing efficiency with a Maxblend impeller in a slurry reactor compared to the A200 (an axial-flow impeller) and the Rushton turbine (a radial-flow impeller). The ERT data was used to evaluation of the particles' distribution inside the reactor and create to profile of gradient particle concentration and the further to assess the degree of homogeneity and mixing index of the suspensions. Analysis of hydrodynamic parameters and the equipment design shown, that use of the vessel with baffles enhanced the degree of homogeneity obtained by the Maxblend impeller for optimal rotor speed and fixed particles content. For this, a rotor was used the best experimental results of solids suspending. In [117,118], the authors performed CFD modelling using the Eulerian and Eulerian (E-E) method, k-ε turbulence model and sliding mesh (SM) technique to analyse the performance of the Maxblend impeller in solid-liquid mixing system as a supplement of study.

2.8. Particle in Three-Phase Reactors. Drawdown of Floating

Flotation, as presented in Figure 3, is a process that uses differences in the surface properties of the solid phase and is commonly used within minerals processing industry [119], waste treatment, electrolyte cleaning and, recently, in the processing of secondary (anthropogenic) raw materials [120]. Depending on the type of process, it is common that three phases (gas-liquid-solid) remain in contact. The effectiveness and efficiency of the flotation process depend on many factors and a number of

parameters closely related and require empirical constants consideration, which indicates the high complexity of the process.

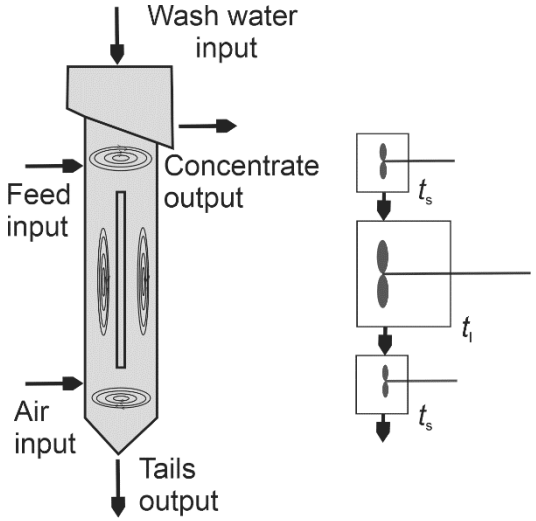

Figure 3. Model of mixing in flotation columns (t_s, t_l denotes process characteristic time).

Flotation is also a mass process, and its direction is determined by a large number of numerous random events. These are three sub-processes involving (1) collision, (2) attachment and (3) detachment [121]. Due to the random character, only the probability of occurrence can be estimated. Thus, describing the subprocesses of flotation by the defined probabilities, which affect the rate of the process the value of flotation rate constant can be evaluated which indicate its relationship with the process parameters and properties of minerals. This value has a macroscopic character and should include information on the factors affecting the flotation process [122–126]. Available in the literature studies shown mainly flotation process, related to minerals flotation, as a fluid flow analysis or as a means of mass transport or as an unsteady process and creating models based on heuristic considerations [123], experimental data or numerical simulations [124]. To predict flotation efficiency and for a research tool, it is required to model flotation that is a multiphase, multi-component and heterogeneous process. Finch and Doby [127], based on experimental results from a mass transfer and hydrodynamic point of view, indicated that the mixing conditions in a multi-chamber flotation chamber could be well described as a continuous perfectly mixed reactor. Likewise, the hight industrial pneumatic flotation columns also operate closer to a single superbly mixed vessel. For a more detailed understanding of operating principles of a particular type flotation and prediction recovery of mineral processing [128], only the most important parameters should be considered, such as the bubbles surface area flux, related to the generation and distribution of the bubble inside of flotation chamber [129,130] as well as the rate of particle collection related to the mass transport across the pulp-froth interface and froth recovery which are primarily related to the gas-phase residence time in the froth [131,132].

The energy required to form a stable suspension of solids (50–150 microns for ores flotation), and to disperse the air as fine bubbles (1–2 mm), is about 1 kW/m^3 for large size of industrial of pneumo-mechanically flotation chambers. Depending on the shape of flotation device, such as being a column, for which a necessary condition for mineral separation in a flotation process is the existence of a froth zone (concentrate) with a distinctive pulp-froth interface was theoretically described by Xu et al. [133] and Langberg and Jameson [134] based on hydrodynamics for two-phase flow air and water system [135,136]. This industrial process has been shown by Yianatos and Henrı'quez [137] as mass transport and stating; that for typical superficial gas rates, J_g 1–2 cm/s, the optimal range of bubble diameter at the pulp/froth interface level was d_B = 1.0–1.5 mm, to maximise bubble surface area flux, S_B = 50–100 1/s. The fundamental models to describe the flotation process, particularly

related to the collection zone in terms of hydrodynamic conditions inside the flotation chamber have been developed for many years; however, still, a number of crucial unsolved issues is very large [138–140]. A general flotation model presents creation [141,142] or disintegration [143,144] of flotation aggregates (bubble–particle) and analyses of the phase particles interaction within a turbulent environment [119,120].

Dispersive of the Gas Phase in the Flotation Chamber

Gas-phase dispersive in the flotation chamber is an essential parameter for this three-phases enrichment process. The power input from the impeller is needed to so that the frequency of particle–bubble collision and attachment was maximised, while at the same time, detachment occurrences are minimised [145]. Too small input of energy will cause some solids to sedimentation as well as not producing sufficient particle–bubble collisions ending to permanent adhesion provide to achieve the desired recovery of the solid phase (see Figure 4), whereas too much energy input will cause breakdown aggregates of particle-bubble and resulting reduction of recovery. The development of computational methods, due to continual improvements in computers and modelling procedures, has become a breakthrough in modelling technological processes, including also flotation.

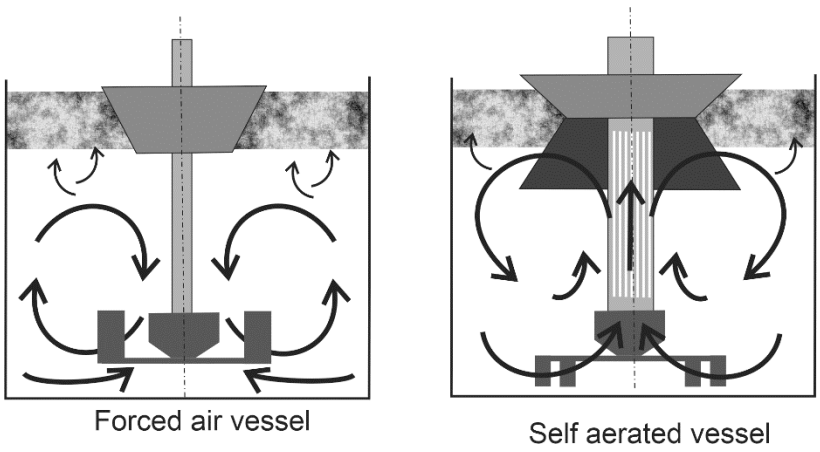

Figure 4. Mechanical flotation chamber.

The advantage with CFD is the possibility to model any tank design at any size, with various flow details, such as internal velocities, shear rates, turbulence parameters, distributions of phases, bubble sizes, particle sizes and residence time distribution, as well as overall quantities, such as power consumption and mixing time [146,147]. There are many additional considerations in modelling methods like CFD, since simulations can have limited accuracy and predictive capabilities of the real process, for example, in cases when the impeller is treated as a 'black box', where the effect of the impeller was modelled using a momentum source or empirically determined boundary conditions. A better approach is the inclusion of the impeller as part of the simulation domain, but while remembering that other limitations exist [148,149]. From another side, the impact of the presence of solid particles on the gas-liquid mass transfer is also of interest. Three mechanisms are analysed of exist solids, which are affecting the gas-liquid mass transfer:

- a viscosity effect, due to damping of the turbulence by the solids [72];
- in the heterogeneous regime, solids have been shown to supplant small bubbles in the dense phases [58,148];
- an interface effect of very tiny particles (either enhance the gas-liquid mass transfer or in some cases hinder it by phenomena coalescence [150–152].

The second of the mechanisms indicated was examined by Scargiali et al. [153]. The authors analysed the results for the Long Draft Tube Self-Ingesting Reactor (LDTSR) dealing with three-phase

(gas-liquid-solid) systems as a "self-ingesting" vessel in which the headspace gas phase is injected and dispersed inside the vessel through surface vortices. Authors found that the impeller pumping capacity and gas-liquid mass transfer coefficient (measured by the Simplified Dynamic Pressure Method (SDPM)) depends on the number of solid particles in the vessel.

2.9. Liquid-Liquid Mixture

Homogenisation of two mutually dissolvable liquids is achieved through convection and molecular diffusion, but circulating can speed up the time when the homogeneous condition reaches. CFD has used to evaluate fluid flow motion as well as to predict the mixing behaviour of the miscible liquid system, e.g., in the mixing of ethanol and glycerol [23], the homogenisation of two mutually dissolvable fluids with different properties [25], the water-ethanol system [26] and the mixing of two miscible liquids with very different viscosities and densities [27,154], and intensity of solid-liquid mixing inside a stirred tank with various impeller layouts [155].

Kamil et al. [156] presented investigation deals with the determination of the minimum agitation speed (N_{cdg}—minimum impeller speed needed for complete liquid-liquid–gas dispersion,), for complete liquid-liquid dispersion in mechanical agitated liquid-liquid mixtures sparged with a gas phase. The minimum impeller speed needed to completely disperse a liquid-liquid system was accurately predicted as the Froude number, by the Skelland and Ramsay correlation [157]. A new correlation is proposed for the prediction of minimum agitation speed, for three-phase (liquid-liquid–gas) system for different volume fractions of the dispersed phase in the form of:

$$Fr_{min} = C^2\left(\frac{T}{D}\right)^{2\alpha} \varphi^{0.106}(G_a - B_o)^{-0.084}(Re_G)^{-0.013} \quad (1)$$

where: F_r—Froude number ($F_r = DN^2\Delta\rho_m g$); C—impeller clearance from tank bottom; D—impeller diameter; T—tank diameter; φ—volume fraction of dispersed phase; G_a—Galileo number ($G_a = \frac{D^3 g\rho_m\Delta\rho}{\mu_m^2}$); B_o—bond number ($B_o = \frac{D^2 g\Delta\rho}{\sigma}$); Re_G—gas Reynolds number.

The calculated minimum Froude number from Equation (1) and obtained experimental data showed excellent agreement with this correlation. Therefore, the authors proposed using the new equation also for other systems and impellers, which are described widely presented in the literature. The flow field analysis inside the stirred vessel at higher rotational speed 1000, 1300 and 1500 rpm, indicated that the three-blade propeller delivers an axial flow direction which is independent of the rotational impeller speed. As a working fluid, they used molasses and water. It has been demonstrated that the gradient of density can be used to determine the time at which ideal mixing is achieved (the homogeneous mixture occurs when the density gradient is zero) [158,159]. On the one hand, the flow pattern causes the water to suppress molasses below impeller so that the molasses can diffuse. The flow pattern inside the stirred tank create unstable loop circulation, so water sucked and diffused with molasses. For this reason, the fluids mixture is sucked and in the axial direction and first enters the propeller then exits the back of the propeller before hitting the bottom wall and changing direction to create a double circulation around the propeller. The author concluded that an indication of the key variables' profiles, such as local velocity, flow pattern, assignation of volume fraction value for liquid of highly viscous, density gradient distribution and criterial numbers for mixing are sufficient to determine the optimal operating conditions for the degree of mixing required.

In [159], the unsteady flow field of the mixing process inside an agitated vessel for different propeller rotational speeds concerning a side-entry configuration, using CFD and the Multiple Reference Frame (MRF) methods, was conducted, as working fluid molasses and water were used, which is a miscible liquid. The process was carried out in the stirred tank with a conical-bottomed cylindrical tank with a diameter T = 0.28 m, and height h = 0.395 m and with a three-blade impeller with a diameter D = 0.036 m. The flow motion formed a non-symmetric double-loop circulation near the propeller with a maximum velocity of 3.83 m/s. The predicted molasses volume fraction value, density gradient and

power number all become time-dependent as well as depending on the propeller rotational speeds under the mixing process while the flow number, increases with the speed of rotation.

2.10. Tomography in Mixing Process

When the global industry is achieves the technological stage 4.0 within manufacturing systems to improve productivity and efficiency, the request for suitable equipment to monitor critical parameters of many processes will appear. Process tomography includes sending a signal through the system and constructing an image based on the signal received across detectors which are arranged a cross-sectional plane of the object. Depending on the type of sensors used, the tomography can be divided into positron emission tomography (PET) [67] nuclear magnetic resonance (NMR), [160], ultrasound tomography (acoustic) [161] and electrical tomography [87,162]. Based on the electrical properties measurement, such as resistance, capacitance, eddy current, permeability, etc., the electrical tomography is further classified into electrical capacitance tomography (ECT) and electrical impedance tomography (EIT), which include the electrical resistance tomography (ERT) as an special case.

ERT is the most attractive method because of its simplicity, high-speed capability and durable construction of the topographer robust to cope with the most industrial environment like chemical engineering processes, including bubble columns [108], solid–liquid filtration, polymerization, phases separation, photoreactors [29] and in the mixing processes [50,87,151,163].

The objective of the ERT system is receipt the resistance and distribution inside vessels. Data can be obtained by applying currents (or voltages) and measuring voltages (or currents) via electrodes installed on the boundary of the domain. A typical ERT system consists of three elements: sensors system, data acquisition system and image reconstruction system/host computer. Each of the components affects the measurement performance, and they are subject to attention. Electrical resistance tomography is a simple, a low cost, high temporal resolution and is also non-intrusive, but it has disadvantages including a low spatial resolution, a complex image reconstruction and sometimes can be invasive.

2.11. The Effect of Impellers

The flow generated by the impeller is influenced by various factors including the geometry and number of impellers [28], the type [29] and size [30] of the impeller, the location and layout of the impeller [31] and rotational speed. Li et al. [162] analysed the flow field characteristics by means of CFD in dual-Rushton turbine stirred vessels at laminar and turbulent regimes. The simulation results showed that flow pattern and dimensionless velocity distribution are related to Reynolds number and regime type without change values in the turbulent regime. The lowest drop of total power number for single and parallel configuration of the impellers was observed in laminar regime [5,6,78,79,164]. A large number of researchers have performed numerical simulations to examine the impact of impeller geometry on the mixing process in order to find optimal configuration, low mixing time or low power consumption [165–167].

3. CFD Simulation of the Mixing Process

The Computational Fluid Dynamics method for the mixing process analysis has developed rapidly in the last three decades. This technique is now an up-and-coming and very useful tool to simulate the mixing process in stirred vessels, including all flow regimes (laminar, transitional and turbulent) as well as single-phase, two and multiphase system.

Numerical methods were gradually developed, to capture detailed information about hydrodynamics and chemical reactions in the agitated vessels. The essential aspects of the numerical analysis involve impeller or tank optimisation, a numerical method for the solution, turbulence and impeller models. The methodology and the governing equation are found to be essential factors that impact accuracy as well as a computational burden. The proper turbulent model may significantly decrease computational requirement and at the same time increase the accuracy of the numerical results. The CFD implementation in the evaluation of liquid-liquid, liquid-solid and gas-liquid concentration

is continuously increasing [168–171]. From this point of view, single-phase and multiphase simulation are now universal and applicable to complex rotating systems with high phases coupling and two-way interactions. Some recent studies developed new models and performed a detailed analysis of particle distribution in liquids [172–174].

Agitated vessel with solid-liquid and gas-liquid phases are recently widely used in engineering processes; however, their modelling and hydrodynamics analysis is still very challenges because of complex, complicated and numbers of various interactions between each phase, walls, baffles and rotating one or more impellers. A large number of researchers have performed valuable investigations in order to better understand the phenomena and the complexity of the flow motion in agitated vessels to better control mixing process [175–177]. Using CFD analysis, the mixing system efficiency for typical small-to-large agitated vessels under real conditions can be evaluated. The number of parameters that CFD simulations can delivery is very large and detailed, and typically includes mixing time, power consumption, flow field pattern, the concentration of phases and flow types. The impeller geometry in reference to vessel geometry is the crucial system component that often determines the efficiency [178,179] of the rotating vessel its design features, as well as the power characteristics [41,180]. The CFD of mechanically agitated vessels was initially implemented for single-phase liquid flow, and for two-dimensional (planar or axisymmetric) geometry [181,182]. With the computer technology increase and modern numerical methods, three-dimensional multiphase transient CFD investigations become now possible [183,184].

In the literature, a large number of studies concentrate on fluid mixing in the laminar or laminar up to transitional flow regimes, in the stirred vessels without the baffles [185,186] or in vessels with baffles even for the laminar creeping flow cases with low Reynolds numbers [187,188]. This direction is very promising because new impellers types are highly required for shear sensitive newly discovery materials in chemical, cosmetics and medical industry.

3.1. Gas-Liquid Phase in CFD

Ranade et al. [189] carried out CFD of the trailing vortices behind rotating impeller using a constant diameter bubble and quasi-steady-state assumption. The presented analysis shows that the turbulent kinetic energy was, for most cases, under predicted [190,191]. The two-phase gas-liquid CFD models developed used the snapshot method. The authors analyse different flow regimes in rotating vessels implemented with Rushton or pitched blade turbines. In this study, only half of the vessel's geometry was taking into account assuming the flow symmetry. The simplified model was inaccurate and not able to properly describe flow behaviour.

Morud et al. [192] show a comparison between CFD analysis and LDA experimental measurements for gas-liquid fluid flow. The authors concluded that gas-phase radial velocity component in the region close to rotating impeller was predicted well; however, axial gas velocity components were over predicted. In similar research studies [193,194] investigated numerically gas-liquid fluid flow vessel taking into account drag force between phases only and assuming constant bubble diameter. It has been shown that the average radial velocity component and velocity fluctuation for gas-phase agreed with experimental measurement, but this means that axial velocity component for gas phase was overestimated. Scargiali et al. [75] analysed gas-liquid fluid motion in an agitated vessel assuming constant bubbles diameter and shape. Despite the assumptions, simplifications and steady CFD simulations results show reasonable agreement with experimental measurement.

Sun et al. [195] performed numerical and experimental analysis for gas hold-up distribution in the stirred vessel. Results showed reasonable agreement in the top tank part and velocity underestimation in part below the impeller. CFD analysis carried out by Khopkar et al. [196] evaluates the impact of flow configurations on gas dispersion in an agitated tank. the authors assume constant bubble diameter and drag force only. An advanced numerical model to evaluated gas hold-up and bubble size distribution in an agitated vessel using population balance equations was shown in [148]. In this research study, one-way coupling was used, and the bubble size was in the range of 0.125–32 mm.

Similar detailed and complex CFD modelling for gas-liquid fluid flow in the agitated vessel was conducted in [197]. The authors predicted bubble size using the bubble number density equation. Transient CFD simulations in a mixing tank with baffles and free surfaces were investigated in [198]. The used numerical model assumes fixed bubbles diameter and constant drag coefficient.

The liquid homogenisation in a gas-liquid baffled cylindrical vessel implemented with pitched-blade impeller was done by Jahoda et al. [199]. In this pseudo-steady state simulation, fixed impeller rotational speed was used with constant bubble diameter and variable gas flow rate. The presented numerical results agree well with experimental measurement. Pinelli et al. [193] investigated two gas-fraction models in two-phase gas-liquid flow. Authors separate gas bubbles into two large groups (large bubbles and small ones). The first group were assumed as a continuous medium during the second one as perfectly mixed.

Wang et al. [200] used CFD simulation to model hydrodynamic characteristics of two-phase gas-liquid fluid flow in an agitated vessel with two impellers. The authors implemented a Multiple Size Group (MSG) model to evaluated bubble size distribution. It was shown that hydrodynamic characteristics, such as bubble size distribution and gas hold-up, could be accurately evaluated by the developed model [201–205]. Industrial applications, require accurate closure models to account for physical behaviour in the scale of small to large scale bubbles, which cannot be fully resolved on an industrial scale. A set, used in the literature, for closure relations was able, with success, to predict bubble motion in columns, including the model extension required to account turbulence and the drag force has been presented in [206–208].

In [209], the drawdown of floating solids process was analysed. Authors performed CFD numerical simulations for two different impellers and four different baffle geometries. It has been concluded that the impeller type and clearance size have a significant impact on drawdown speed of floating solids in an agitated vessel. Results show high particle concentration in the vicinity of the shaft just above the for Rushton turbine. It was presented that for analysed turbines, a larger clearance result to a higher drawdown rate of floating solids occurred. In general, air bubbles, coalescence or break-up in the gas-liquid mixture are extremely difficult to model in a selected number of research studies; these complex situations were investigated [210].

The critical impeller speed for solid suspension in the gas-liquid-solid stirred reactor was investigated using steady-state CFD analysis in [211]. The simulations were done under different operating conditions and with a fixed bubble size of 3 mm. In similar studies [212,213] gas-solid-liquid three-phase flows analysis was carried out showing the ability to solve very complex mixing problem. A mass transfer analysis for the three-phase gas-liquid-liquid stirred tank reactor was done by Gakingo et al. [212]. The authors, with success, applied CFD modelling to small scale industrial problem.

3.2. Mixing System Optimisation

In order to optimise reactor design as well as impeller-tank mixing system and to obtain optimal yield and selectivity, appropriate models' turbulence and the mass transport model in the vessel are critical issues [214]. Due to the scale problem and the physical complexity, the mixing process optimisation remains a complicated problem. Recently, CFD modelling has been employed to analyse multiphase flow mixing in various configurations and in order to optimise the whole system including various reactors, bio-reactors and chemical reactors. Multiphase mixing optimisation may occur in the case of liquid-liquid mixing [215] for Newtonian and non-Newtonian fluids [89,163,216]. The development in CFD tool makes it a very good alternative in process design and optimisation, including complex hydrodynamics analysis, chemical reactions and heat and mass transfer. In the last decade, in a number of research studies on impeller and tank shape, as well as the whole process, parametrisation has significantly grown [217–220]. In the current literature, CFD simulation is integrated with various widely available optimisation algorithms [204,221–223] including heuristic, genetic algorithm, neural network.

Because of the large complexity of the agitated vessel, the selection of efficient optimisation algorithms is crucial. Often to improve the computational performance, hybrid methods are implemented [224], which account for two or more optimisation algorithms [225], even though very large number of runs is usually required making optimisation process non-trivial [226,227]. An optimisation of continuous stirred-tank for hydrogen production using CFD was conducted in [228], where the authors performed 3D CFD analysis, assuming biogas with bubble mean diameter equal to 1 mm. The presented analysis has shown that the most suitable impeller speed for hydrogen production is in the range 50–70 rpm.

Impact of shape design and tank-impeller configuration were analysed and optimised with success using CFD in many research works [229–231]. Some analyses also take into account the effect of impeller diameter on Nusselt number and power dissipation. In [232–234], the authors show with success that using a recently developed method impeller performance or whole system optimisation become possible. It was also found that flat-bottomed vessels dissipated about 15% less power in reference to the hemispherical-bottomed vessel. For this reason, the total power dissipated in the hemispherical-bottomed vessel to suspend the particles was about 50% higher than for the tank with a flat bottom. This shows large potential in mixing systems optimisation to decrease the amount of required energy. Often, the optimisation results can be directly applied to the industrial systems.

Liquid-solid particle dispersion and mixing process optimisation were studied in [235]. The authors applied the Euler-Lagrange approach and one-way coupling. It was found that for low-density ratio, analysed configurations produced good quality mixture over the wide Stokes number range. Meanwhile for high-density ratios, the lifted shape generates a much better mixing quality. The fastest mixing was obtained due to the established high exit velocities by the bottom configurations where the tripod is installed at the lowest part of the vessel. In a similar research work [236], Eulerian-Lagrangian analyses of settling and agitated dense solid-liquid suspensions were conducted.

3.3. Mass Transfer with CFD

Mass transfer in agitated viscous shear-thinning dispersions using CFD modelling, taking into account population balance, was conducted in [237]. In numerical research studies, the mixer geometry was considered as an axisymmetric, and only half of the vessel geometry was analysed. The authors found that the largest mass transfer was located in small bubbles. Kordouss et al. [237] predicted a two-phase mass transfer coefficient in the agitated tank using computer simulation. The authors used a stirred tank with 45° pitched blade impeller; bubbles diameter was in the range 0.75–12 mm, and they were divided into 13 groups. It has been shown that the multi-size bubble method shows much better prediction in reference to the method with only the one average bubble diameter assumption. Hydrodynamics and mass transfer in a stirred tank is an important issue and was analysed with success by many researcher groups [238–242]. Gimbun et al. [243] investigated a hybrid method composed of CFD and population balanced technique to model mass transfer in gas-liquid rotating vessels with CD-6 and Rushton turbine. The authors show that, using a hybrid method, bubble size distribution was much more accurate than using a uniform bubble diameter. However, the proposed model failed to create a detailed evaluation concerning bubbles diameter and discretisation. Laakkonen [244,245] developed a new method called “multiblock”, in which population balance for bubbles was implemented to calculate local bubble distribution. Bubbles were divided into a number of small sub-regions and divided into a large number of groups. The authors found that the proposed model performed better than models which based on fixed bubble diameter. Mass transfer in correlation to diffusion-controlled corrosion at the outer surface of coils immersed in rotating tank was analysed in [246].

The impact of power input on gas-liquid mixing efficiency and mass transfer for bioreactors was analysed in detail in [247]. The authors applied the electrical method to measure the specific power input into a disposable bioreactor. It was shown that the power peak influences the operational parameters of the mixer. The mass transfer coefficient for gas-liquid oxygen was correlated with the peak power input, confirming that the mass transfer increased significantly with specific power

value. Energy requirement due to mixing process and mass transfer in a photobioreactor was analysed in [248]. The authors show that wave bioreactors have large potential and are able to obtain very high mixing rates with low shear stress. They are also able to create high gas-liquid mass transfer without sparging what is crucial for many industrial processes.

3.4. CFD Models any Turbulence in Rotary Mixers

Computer simulations, in many cases, can replace the need for the time-consuming and problematic to performed laboratory-scale experiments. Their performance and ability to provide good results were verified for a wide variety of configurations. At present three main approaches have been used to model turbulent flow motion in an agitated vessel: RANS (Reynolds averaged Navier–Stokes), the LES (large eddy simulation) and the DNS (direct numerical simulation). The most widely used model for the moving boundaries problem is at present still RANS model. For engineering problems [249,250] the RANS model is much more computationally economic in reference to LES and much faster than DNS. The most accurate results can be obtained using DNS, where the instantaneous flow variables are obtained directly by solving unsteady 3D Navier–Stokes equations, and no additional models are required [171,172,251–253]. However, this method requires very large computational resources and is still beyond engineering applications or unpractical for industrial application and is limited to simple geometry and low Reynolds number. For this reason, for detailed analysis, Large Eddy Simulation is often used because required less computational resources. [254–258]. In LES method only large scales are fully resolved similarly to DNS, but the smallest scales due to much lower grid resolution than for DNS have to be modelled using one of the widely available turbulence models.

In recent years, the Direct Numerical Simulation and Large Eddy Simulation models have been applied into the numerical investigation for agitated vessel; although the results are very accurate and excellent in reference to the experimental data, it requires tremendous computational cost which makes these methods not acceptable in real applications [259,260]. Another possibility is the Detached Eddy Simulation (DES) which requires less CPU resources but is still rarely used for of turbulent flow modelling in stirred tank reactor [261]. Figure 5 shows the scheme of the turbulence model classification.

The commonly used RANS modelling solved the averaged fluid flow equations, and for this reason, an additional appropriate turbulence model is required. In the literature, a large number of turbulence models for rotating vessels with single or more impellers and with or without baffles can be found [262,263]. Each turbulence models used has advantages as well as disadvantages. In the literature, the authors proposed different turbulence models depending on particular cases, or even recommended different models for identical configuration [262–264].

One can infer from the literature review that to calculate multiphase flow in rotating vessels, mainly the k-ε models have been used. This group of models generally gives good agreement with experimental data for the average velocity in the bulk region; however, it overpredicts the average radial and tangential velocity components in the area close to the impeller as well as underestimates velocity fluctuations and the kinetic energy of turbulence [260]. The literature analyses [263,264] show that RANS simulations in reference to more detailed LES method for identical vessels and impeller configuration underpredict energy dissipation by about 20–25% [265], or in some cases as much as 45% [266,267]. On the other hand, some authors reported similar results for RANS and LES [199]. The difference between results for similar simulation performed using RANS only are also significant ranging from poor turbulent prediction even in single-phase systems. This is still a crucial issue, to have appropriate and accurate results of stirred tanks simulations for multiphase flows [196,268,269]. The errors and uncertainties of numerical simulations are usually related to modelling deficiencies only, and the numerical errors should not be disregarded in the validation [270].

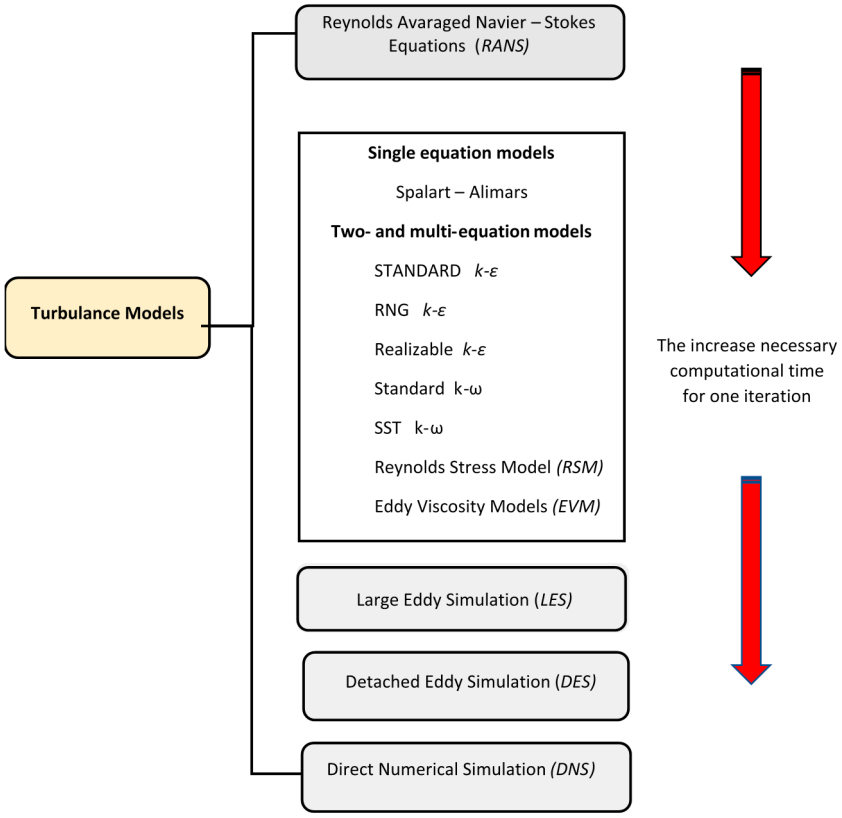

Figure 5. Turbulence models classification.

Numerical schemes and numerical issues are as important as the turbulent mode [196,267]. The dependency of turbulent models on numerical consideration for agitated vessels with impeller has been faced only in a very limited number of research studies. Due to technical limitations in the past, mixers were usually solved with low grid resolutions [145,271,272]. The recent availability of very powerful clusters and multi-core workstations allows the conduction of systematic research studies on the evaluation of the numerical error with respect to the models' assumptions and approximations. Regarding such analysis, there is the impact of the rotating reference frame size on flow in the case of the straight-blade impeller in a baffled stirred tank [273]. In the selected works [274,275], presented in the literature, attention is paid on the impact of the turbulent model closure and near-wall region treatment on the accuracy of the most widespread RANS method for agitated tank with impeller [276,277].

RANS shortcomings are due to the isotropic nature of eddy viscosity models and can be defeated using any anisotropic models, for example, the Reynolds Stress Model. Fluid flows around the impeller comparisons between RANS and LES, but for single-phase flows shows that [255,264,270], RANS or URANS (unsteady RANS) are able to resolve the general flow field; however, LES is required in order to get a very agreement with the turbulent structures in the area close to the impeller [180,255,260,265,270]. A recent comparison of RANS /URANS and LES has led to state that the LES is more accurate into flow field prediction [270,278,279]; however, different conclusions about turbulence prediction are drawn by different authors [280,281].

For the flow with particles, i.e., flows with continuous phase and discrete phase, three common ways, are used in which the non-continuous phase can be introduced to the turbulence models. Typically using the dispersed models, the continuous phase turbulence is model using additional equations, for example, for k and ε, and the dispersed phase are turbulence parameters are calculated based on continuous phase parameters [198,204,282]. In the case of the mixture model, equations are used directly for the fluid multiphase mixture in order to obtain kinetic energy of turbulence and Reynolds stresses [283–287]. Finally, the presented solution proposes model equations for each phase

separately. As can be seen from literature data, the mixture and dispersed models are widely used in research studies related to the fluid mixing using agitated vessels.

In the case of flow with particle or bubbles, the implementation of the key force is crucial for proper modelling [287]. Among many forces, drag force has been assumed to be essential while additional forces, i.e., lift force, added mass, Magnus force and turbulent dispersion force are usually neglected but often without justification. Additional forces implementation is laborious task [282,287,288]; even for the commonly used drag force, a large number of correlations can be found in the literature [209]. In particular, to properly evaluate the bubble size distribution break-up as well as bubble coalescence model need to be developed. However, up to now, neither the physical phenomena nor accurate way of modelling is not known, and bubble behaviour models are limited to simple cases [183]. For two- and more phase flow applications, typically Euler-Euler and Euler-Lagrange frameworks are used to couple the different phases together.

3.5. Impeller Rotation Modelling

A curial aspect to consider when running CFD simulations of the stirred vessel with or without baffles is the way of modelling impeller or vessel. In the literature, different approaches have been developed and implemented [289–291]. Impeller or mixing tank motion poses a challenge because some parts or whole domain are moving relative to the tank or baffles wall. The first techniques developed to solve this issue was impeller boundary condition [289] and imposed source or sink terms [182,290]. In some research studies, the method called snapshot was used with success even for gas-liquid fluid flow analysis in an agitated vessel with baffles [291]. In the past, fluid motion simulations in a rotating tank have been performed with a so-called 'black box' approach, and the impeller area was usually removed or excluded from the analysed domain [292]. However, in most of the simple methods proposed in the past, detailed boundary conditions about velocity and turbulence need to be specified on the volume or surface sweep by the rotating blades. This information about boundary conditions can only be obtained from experimental measurement [293,294]. For this reason, new methods which do not require data from experimental measurement were developed.

The most popular methods for an agitated vessel with and without baffles are at present sliding mesh technique (SM) [40,295] (the similar technique was adopted in [296]) for the fluid flow simulation of blade turbine. In this technique, the vessel is divided into two sections, the first containing impeller and second the volume of fluid also tank walls and baffle if required. The whole computational mesh in the impeller section rotates with the same rotational speed as impeller while mesh in vessel section is stationary. The sliding mesh technique does not need any data from experimental measurement, but from the computational point of view, this approach is very expensive for start-up calculation and is not recommended for optimisation simulations [297]. To avoid this, a different drawback approach called multiple reference frame technique (MRF) was investigated [298,299]. In this technique, the agitated tank is divided into two or more (or single in single reference frame) frames—stationary frames and moving frames. The stationary frame includes the tank, baffle if requires and whole flow outside moving frame while the moving reference frame includes only the impeller and the flow enclosed in this area [296]. From comparisons of SG and MRF, the second technique has much higher computational performance [146]. The MRF and snapshot model are steady-state models; however, the MRF model is often used by a large number of researches in comparison to other [274,300]. Unfortunately, the snapshot model is not able to consider interactions between impeller and baffles which significantly impact the accuracy of numerical simulation. On the other hand, the Multiple Reference Frame model accurately accounts for this type of interactions dividing the domain into rotating stationary zone with baffles and rotating zone with the impeller.

It is clear that the MRF method is more computational in reference to the SM method due to its steady-state consideration and decreases computational time about one order of magnitude [301]. In many cases, this method generates very similar results [302] in all flow regimes [175,188,302–304]. For rotating vessel operating at transitional and turbulent flow regime [303] it has been pointed out in

the literature that the size of Stationary Reference Frame (SRF) and Rotating Reference Frame (RRF) in the MRF method is not arbitrary and can significantly influence the numerical results. The interface, which is crucial, should always be located in the region where flow variables gradient is low on the other word close to zones interface flow variable cannot change rapidly, neither in angular direction nor in time. Some authors recommended that the radial distance between the interfaces should be located in the midway between the vessel wall or baffles and impeller edge [305–309]. The authors performing the CFD simulations for the MRF interface located about one impeller radius above and below radial flow Rushton impeller found an impact of interface position on the angular velocity profile. It has been noticed that for the axial flow, the high gradient may occur at a larger distance. For this reason, in some studies [300], the recommendation is to extend rotating zone approximately one to four impeller radius above and below the impeller. Depending on the authors, the interface between rotating and stationary frame should be located 0.5 impeller radius R from the impeller tip and approx 1.5 impeller blade widths above and below the impeller centreline. Other researchers set the zones interface at the axial location about 0.5 radius above and below impeller, while the radial distance was set at 1.5 impeller radius [67]. In [272], the authors evaluated four various cylindrical zones around the impeller by varying axial (in the range 0.62 R up to 1.27 R) and radial (in the range 1.11 R up to 1.43 R) distance from the impeller. The researchers conclude that in order to perform reliable CFD simulation, the rotating zone has to include the locations where the flow motion shifts from accelerating to decelerating. In [269], it has been found that at the very low Reynolds number MRF interface location has no significant impact in the results, but it starts to play a significant role when the Reynolds number raises above 29.4. According to various studies [67,269,272,300] the size of the rotating domain dependents on the fluid flow regime and for higher Reynolds number RRF has to be enlarged. Authors also found that numerical results for velocity vector and power number are more sensitive to the size of the rotating reference frame than to the mesh resolution. Additional information about numerical modelling approach, turbulence models and numerical scheme and issue related to the rotating frame can be found in [217,309].

4. Conclusions

This review has been carried out on the current development of mechanically agitated vessels. The application and development of modern experimental methods and the computational fluid dynamics techniques to simulate the mixing process were presented. The CFD tool, which is based on the fundamental principles of transport phenomena, recently became excellent in fluid flow and mixing parameters predictions in the case of single-phase and multiphase problems. The modern multi-point and planar experimental techniques have become a standard today in research progress, ranging from the simple ones which rely on visual observation to sophisticated ones encompassing special equipment (LDA, PIV, LIF), sensors and software.

At present, many methods are available for flow pattern visualisation in mixed vessels. However, all-optical methods required optical access. The CFD modelling technique has gradually developed to capture detailed information about hydrodynamics and chemical reactions in the agitated vessels. The CFD tools implementation in the evaluation of liquid-liquid, liquid-solid and gas-liquid concentration is steadily increasing. From this point of view, single-phase and multiphase simulation are now applicable to complex rotating systems with phase coupling and four-way interactions. Recent studies presented here developed new models and performed a detailed analysis of fluid flow mixing in vessels. Still, for complex phenomena, numerical models are not able to predict flow mixing property, or they required empirical data not always available in the literature. The explanation of the mechanism of suspension formation in a mixing system still needs to be elaborated, indicating the reasons for the difference for suspension without gas and with the gas solution. Problems with chemical reactions and more than one impeller or aerator are still a challenge.

Author Contributions: Conceptualisation, M.J.; methodology M.J. and A.M.; supervision, M.J.; writing original draft and editing, M.J. and A.M. All authors have read and agreed to the published version of the manuscript.

Funding: The present work was supported by the Polish Ministry of Science (Grant AGH No. 16.16.210.476) and (Grant AGH No. 16.16.100.215).

Conflicts of Interest: The authors declare no conflict of interest.

Nomenclature

a	gas-liquid interfacial area, m^2
C	impeller off-bottom clearance, m
D	impeller diameter, m
d_p	particle size or particle diameter, μm
d_S	diameter of the sparger ring, m
H	liquid height in the vessel, m
T	tank diameter, m
V	tank volume, m^3
h	distance between the agitator and bottom of the vessel, m
A	height of the agitator blade, m
B	width of the agitator blade, m
B_o	Bond number ($Bo = D^2 g \Delta\varrho/\delta$)
C_b	bed packing coefficient, *v*/*v*
C_v	solids volume concentration, *v*/*v*
$(C_v)_{max}$	maximum solids concentration, upper limit, *v*/*v*
C_{vb}	solids packing volume concentration (*v*/*v*)
Fr	Froude number ($Fr = DN^2\varrho_m\Delta\varrho g$)
G_a	Galileo number ($G_a = D^3 g\varrho_m\Delta\varrho/\mu^2_m$)
H_o	dimensionless homogeneity index/degree
J_g	superficial gas rates, cm/s
$k_L a$	volumetric mass transfer coefficient at the gas-liquid interface, s^{-1}
L	length of the baffle, m
M_S	mass of solids, kg
MI	mixing index
N	impeller speed, rps
N_{cdg}	minimum impeller speed needed for complete liquid-liquid–gas dispersion
N_H	homogenization speed, rpm
N_{js}	minimum impeller speed required for just complete off-bottom suspension of solids under un-gassed conditions, rps
N_{jsg}	minimum impeller speed required for just complete off-bottom suspension of solids under gassed conditions, rps
P	power consumption under un-gassed condition, W
P_{js}	agitator power for just-off-bottom solids suspension, W
Re_G	gas Reynolds number
Re_E	Reynolds number of turbulent eddies at N_{js}
S_B	bubble surface area flux, s^{-1}
t_H	homogenisation time, s
t_m	mixing time, s
w	width of the baffle, m
$\Delta\varrho$	density difference between solid and liquid, kg/m^3
φ	gas hold-up
X	Zweitering solids loading, *w*/*w*
X_v	volume solids fractions, dim
ε_{js}	agitator power per unit solids mass at the just-off-bottom solids suspension condition, W/kg
μ	viscosity, Pa.s

References

1. Schrimpf, M.; Esteban, J.; Rosler, T.; Vorholt, A.J.; Leitner, W. Intensified reactors for gas-liquid-liquid multiphase catalysis: From chemistry to engineering. *Chem. Eng. J.* **2019**, *372*, 917–939. [CrossRef]
2. Major-Godlewska, M.; Karcz, J. Power consumption for an agitated vessel equipped with pitched blade turbine and short baffles. *Chem. Zvesti.* **2018**, *72*, 1081–1088. [CrossRef] [PubMed]
3. Lampinga, S.R.; Zhanga, H.; Allenb, B.; Ayazi, S.P. Design of a prototype miniature bioreactor for high throughput automated bioprocessing. *Chem. Eng. J.* **2003**, *58*, 747–758. [CrossRef]
4. Młynarczykowska, A.; Simone, F.S.; Demurtas, L.; Jaszczur, M. Impact of baffle geometry on the fluid motion in the stirred vessel. In Proceedings of the EFM, Experimental Fluid Mechanics Conference, Franzensbad, Czech Republic, 19–22 November 2019; pp. 321–326.
5. Młynarczykowska, A.; Simone, F.S.; Demurtas, L.; Jaszczur, M. An experimental investigation on the fluid flow mixing process in agitated vessel. In Proceedings of the EFM, Experimental Fluid Mechanics Conference, Franzensbad, Czech Republic, 19–22 November 2019; pp. 321–326.
6. Jaszczur, M.; Młynarczykowska, A.; Demurtas, L. An experimental and numerical analysis of the fluid flow in a mechanically agitated vessel. In Proceedings of the XII International Conference on Computational Heat, Mass and Momentum Transfer (ICCHMT 2019), Rome, Italy, 3–6 September 2019; Volume 128, p. 15.
7. El-Gayar, D.A.; Konsowa, A.H.; El-Taweel, Y.A.; Farag, H.A.; Sedahmed, G.H. Intensification of the rate of diffusion controlled catalytic and electrochemical reactions in a new stirred tank reactor with a multicylindrical blade impeller. *Chem. Eng. Res. and Design.* **2016**, *109*, 607–617. [CrossRef]
8. Mishra, P.; Ein-Mozaffari, F. Using computational fluid dynamics to analyze the performance of the Maxblend impeller in solid-liquid mixing operations. *Int. J. Multiph. Flow* **2017**, *91*, 194–207. [CrossRef]
9. Zych, M.; Hanus, R.; Vlasák, P.; Jaszczur, M.; Petryka, L. Radiometric methods in the measurement of particle-laden flows. *Powder Technol.* **2017**, *318*, 491–500. [CrossRef]
10. Hanus, R.; Zych, M.; Jaszczur, M.; Szlachta, A.; Golijanek-Jędrzejczyk, A. Signal processing in the investigation of two-phase liquid-gas flow by gamma-ray absorption. In Proceedings of the 6th International Conference on Control, Decision and Information Technologies, Paris, France, 23–26 April 2019; pp. 681–684.
11. Hanus, R.; Zych, M.; Petryka, L.; Jaszczur, M.; Hanus, P. Signals features extraction in liquid-gas flow measurements using gamma densitometry. In Proceedings of the EFM15 Experimental Fluid Mechanics, Prague, Czech Republic, 17–20 November 2015.
12. Mavros, P. A Review of Experimental Techniques. *IChemE* **2001**, *79*, A.
13. Laakkonen, M.; Honkanen, M.; Saarenrinn, P.; Aittamaa, J. Local bubble size distributions, gas–liquid interfacial areas and gas holdups in a stirred vessel with particle image velocimetry. *Chem. Eng. J.* **2005**, *109*, 37–47. [CrossRef]
14. Jardón-Pérez, E.L.; Amaro-Villeda, A.; González-Rivera, C.; Trápaga, G. Introducing the Planar Laser-Induced Fluorescence Technique (PLIF) to Measure Mixing Time in Gas-Stirred Ladles. *Metall. Mater. Trans. B* **2019**, *50*, 2121–2133.
15. Lau, Y.; Deen, N.; Kuipers, J. Development of an image measurement technique for size distribution in dense bubbly flows. *Chem. Eng. Sci.* **2013**, *94*, 20–29. [CrossRef]
16. Kracíka, T.; Retříčekab, T.; Mouchaa, T. Mass transfer in coalescent batch fermenters with mechanical agitation. *Chem. Eng. Res. Des.* **2020**, *160*, 587–592. [CrossRef]
17. Aubin, J.; Mavros, P.; Fletcher, D.F.; Bertrand, J.; Xuereb, C. Effect of axial agitator configuration (up-pumping, down-pumping, reverse rotation) on flow patterns generated in stirred vessels. *Chem. Eng. Res. Des.* **2001**, *79*, 845–856. [CrossRef]
18. Guida, A.; Nienow, A.W.; Barigou, M. The effects of the azimuthal position of the measurement planeon the flow parameters determined by PIV within a stirred vessel. *Chem. Eng. Sci.* **2010**, *65*, 2454–2463. [CrossRef]
19. Sher, F.; Sajid, Z.; Tokay, B.; Khzouz, M.; Sadiq, H. Study of gas–liquid mixing in stirred vessel using electrical resistance tomography. *Asia Pac. J. Chem. Eng.* **2016**, *11*, 855–865. [CrossRef]
20. Patel, D.; Ein-Mozaffari, F.; Mehrvar, M. Tomography images to analyze the deformation of the cavern in the continuous-flow mixing of non-Newtonian fluids. *AIChE J.* **2014**, *60*, 315–331. [CrossRef]
21. Fitzpatrick, J.J.; Gloanec, F.; Michel, E.; Blondy, J.; Lauzeral, A. Application of mathematical modelling to reducing and minimising energy requirement for oxygen transfer in batch stirred tank bioreactors. *Chem. Eng.* **2019**, *3*, 1–21.

22. Jaszczur, M.; Młynarczykowska, A.; Demurtas, L. Effect of impeller design on power characteristics and Newtonian fluids mixing efficiency in a mechanically agitated vessel at low Reynolds numbers. *Energies* **2020**, *13*, 640. [CrossRef]
23. Al-Qaessi, F.; Abu-Farah, L. Prediction of Mixing Time for Miscible Liquids by CFD Simulation in Semi-batch and Batch Reactors. *Eng. Appl. Comp. Fluid Mech.* **2014**, *3*, 135–146. [CrossRef]
24. Daryus, A.; Siswantara, A.I.; Darmawan, S.; Gunadi, G.G.R.; Camalia, R. CFD Simulation of Turbulent Flows in Proto X-3 Bioenergy Micro Gas Turbine Combustor using STD k-e and RNG k-e Model for Green Building Application. *Int. J. Technol.* **2016**, *7*, 204–211. [CrossRef]
25. Derksen, J.J. Blending of Miscible Liquids with Different Densities Starting from a Stratified State. *Comp. Fluids* **2011**, *50*, 35–45. [CrossRef]
26. Orsi, G.; Roudgar, M.; Brunazzi, E.; Galletti, C.; Mauri, R. Water–Ethanol Mixing in T-shaped Microdevices. *Chem. Eng. Sci.* **2013**, *95*, 174–183. [CrossRef]
27. Montante, G.; Coroneo, M.; Pagliantic, A. Blending of miscible liquids with different densities and viscosities in static mixers. *Chem. Eng. Sci.* **2016**, *141*, 250–260. [CrossRef]
28. Muharam, Y.; Kurniawan, A. Computational Fluid Dynamic Application in Scale-up of a Stirred-batch Reactor for Degumming Crude Palm Oil. *Int. J. Technol.* **2016**, *7*, 1344–1351. [CrossRef]
29. Zhao, J.; Gao, Z.; Bao, Y. Effects of the Blade Shape on the Trailing Vortices in Liquid Flow Generated by Disc Turbines. *Chin. J. Chem. Eng.* **2011**, *19*, 232–242. [CrossRef]
30. Sossa-Echeverria, J.; Taghipour, F. Computational Simulation of Mixing Flow of Shear Thinning Non-Newtonian Fluids with Various Impellers in a Stirred Tank. *Chem. Eng. Proc. Process Intensif.* **2015**, *93*, 66–78. [CrossRef]
31. Rahimi, M. The Effect of Impellers Layout on Mixing Time in a Large-scale Crude Oil Storage Tank. *J. Petroleum Sci. Eng.* **2005**, *46*, 161–170. [CrossRef]
32. del Pozo, D.F.; Liné, A.; Van Geem, K.M.; Le Men, C.; Nopens, I. Hydrodynamic analysis of an axial impeller in a non-Newtonian fluid through particle image velocimetry. *AIChE J.* **2020**, *66*, 6939.
33. Abdulrasaq, U.K.; Ayranci, I. The effect of hydrodynamic parameters on the production of Pickering emulsions in a baffled stirred tank. *AIChE J.* **2019**, *65*, e16691.
34. Tsabet, È.; Fradette, L. Effect of the properties of oil, particles, and water on the production of Pickering emulsions. *Chem. Eng. Res. Des.* **2015**, *97*, 9–17. [CrossRef]
35. Sk, A.A.; Kumar, P.; Kumar, S. Effect of impeller diameter on Nusselt number in mechanically agitated vessel. *Int. J. Num. Meth. Heat Fluid Flow.* **2020**, *30*, 2225–2235. [CrossRef]
36. Jafari, R.; Tanguy, P.A.; Chaouki, J. Experimental investigation on solid dispersion, power consumption and scale-up in moderate to dense solid–liquid suspensions. *Chem. Eng. Res. Design* **2012**, *90*, 201–212. [CrossRef]
37. Sharma, R.N.; Shaikh, A.A. Solids suspension in stirred tanks with pitched blade turbines. *Chem. Eng. Sci.* **2003**, *58*, 2123–2140. [CrossRef]
38. Ayranci, I.; Machado, M.B.; Madej, A.M.; Derksen, J.J.; Nobes, D.S.; Kresta, S.M. Effect of geometry on the mechanisms for off-bottom solids suspension in a stirred tank. *Chem. Eng. Sci.* **2012**, *79*, 163–176. [CrossRef]
39. Ayranci, I.; Ng, T.; Etchells, A.W.; Kresta, S.M. Prediction of just suspended speed for mixed slurries at high solids loadings. *Chem. Eng. Res. Des.* **2013**, *91*, 227–233. [CrossRef]
40. Bakker, A.; Laroche, R.D.; Wang, M.H.; Calabrese, R.V. Sliding mesh simulation of laminar flow in stirred reactors. *Trans. Inst. Chem. Eng. Res. Des.* **1997**, *75*, 42–44. [CrossRef]
41. Ibrahim, S.; Wong, S.D.; Baker, I.F.; Zamzam, Z.; Sato, M.; Kato, Y. Influence of geometry and slurry properties on fine particles suspension at high loadings in a stirred vessel. *Chem. Eng. Res. Des.* **2015**, *94*, 324–336. [CrossRef]
42. Ibrahim, S.; Nienow, A.W. The effect of viscosity on particle suspension in an aerated stirred vessel with different impellers and bases. *Chem. Eng. Commun.* **2009**, *197*, 434–454.
43. Ibrahim, S.; Nienow, A.W. Comparing impeller performance for solid suspension in the transitional flow regime with Newtonian fluids. *Chem. Eng. Res. Des.* **1999**, *77*, 721–727. [CrossRef]
44. Ibrahim, S.; Nienow, A.W. Particle suspension in the turbulent regime-The effect of impeller type and impeller/vessel configuration. *Chem. Eng. Res. Des.* **1996**, *74*, 679–688.
45. Ayranci, I.; Kresta, S.M. Design rules for suspending concentrated mixtures of solids in stirred tanks. *Chem. Eng. Res. Des.* **2011**, *89*, 1961–1971. [CrossRef]

46. Ayranci, I.; Kresta, S.M. Critical analysis of Zwietering correlation for solids suspension in stirred tanks. *Chem. Eng. Res. Des.* **2013**, *92*, 413–422. [CrossRef]
47. Hosseini, S.; Patel, D.; Ein-Mozaffari, F.; Mehrvar, M. Study of solid–liquid mixing in agitated tanks through electrical resistance tomography. *Chem. Eng. Sci.* **2010**, *65*, 1374–1384. [CrossRef]
48. Hosseini, S.; Patel, D.; Ein-Mozaffari, F.; Mehrvar, M. Study of solid-liquid mixing in agitated tanks through computational fluid dynamics modeling. *Ind. Eng. Chem. Res.* **2010**, *49*, 4426–4435. [CrossRef]
49. Harrison, S.T.; Stevenson, R.; Cilliers, J.J. Assessing solids concentration homogeneity in Rushton-agitated slurry reactors using electrical resistance tomography (ERT). *Chem. Eng. Sci.* **2012**, *71*, 392–399. [CrossRef]
50. Tamburini, A.; Cipollina, A.; Micale, G.; Brucato, A. Dense solid-liquid suspensions in top-covered unbaffled stirred vessels. *Chem. Eng. Trans.* **2011**, *24*, 1441–1446. [CrossRef]
51. Tamburini, A.; Cipollina, A.; Micale, G.; Brucato, A.; Ciofalo, M. CFD simulations of dense solid-liquid suspensions inbaffled stirred tanks: Prediction of suspension curves. *Chem. Eng. J.* **2011**, *178*, 324–341. [CrossRef]
52. Tamburini, A.; Cipollina, A.; Micale, G.; Brucato, A. Measurements of N_{js} and power requirements in unbaffled bioslurry reactors. *Chem. Eng. Trans.* **2012**, *27*, 343–348.
53. Tamburini, A.; Brucato, A.; Busciglio, A.; Cipollina, A.; Grisafi, F.; Micale, G.; Scargiali, F.; Vella, G. Solid-liquid suspensions in top-covered unbaffled vessels: Influence of particle size, liquid viscosity, impeller size, and clearance. *Ind. Eng. Chem. Res.* **2014**, *53*, 9587–9599. [CrossRef]
54. Lamberto, D.J.; Alvarez, M.M.; Muzzio, F.J. Experimental and computational investigation of the laminar flow structure in a stirred tank. *Chem. Eng. Sci.* **1999**, *54*, 919–942. [CrossRef]
55. Wu, J.; Zhu, Y.G.; Pullum, L. Suspension of high concentration slurry. *AIChE* **2002**, *48*, 1349–1352. [CrossRef]
56. Kraume, M. Mixing Time in Stirred Suspensions. *Chem. Eng. Technol.* **1992**, *15*, 313–318. [CrossRef]
57. Bujalski, W.; Takenaka, K.; Paolilni, S.; Jahoda, M.; Paglianti, A.; Takahashi, A.; Nienow, A.W.; Etchells, A.W. Suspensions and liquid homogenisation in high solids concentration stirred chemical reactors. *Trans. IChemE* **1999**, *77*, 241–247. [CrossRef]
58. Kuzmani, N.; Zaneti, R.; Akrap, M. Impact of floating suspended solids on the homogenisation of the liquid phase in dual-impeller agitated vessel. *Chem. Eng. Process.* **2008**, *47*, 663–669. [CrossRef]
59. Mishra, P.; Ein-Mozaffari, F. Using tomograms to assess the local solid concentrations in a slurry reactor equipped with a Maxblend impeller. *Powder Technol.* **2016**, *301*, 701–712. [CrossRef]
60. Kazemzadeh, A.; Ein-Mozaffari, F.; Lohi, A. Effect of impeller type on mixing of highly concentrated slurries of large particles. *Particuology* **2020**, *50*, 88–99. [CrossRef]
61. Kazemzadeh, A.; Ein-Mozaffari, F.; Lohi, A. Hydrodynamics of solid and liquid phases in a mixing tank containing high solid loading slurry of large particles via tomography and computational fluid dynamics. *Powder Technol.* **2020**, *360*, 635–648. [CrossRef]
62. Kazemzadeh, A.; Ein-Mozaffari, F.; Lohi, A.; Pakzad, L. Effect of the rheological properties on the mixing of Herschel-Bulkley fluids with coaxial mixers: Applications of tomography, CFD, and response surface methodology. *Can. J. Chem. Eng.* **2016**, *94*, 2394–2406. [CrossRef]
63. Kazemzadeh, A.; Ein-Mozaffari, F.; Lohi, A.; Pakzad, L. Investigation of hydrodynamic performances of coaxial mixers in agitation of yield pseudoplastic fluids: Single and double central impellers in combination with the anchor. *Chem. Eng. J.* **2016**, *294*, 417–430. [CrossRef]
64. Kazemzadeh, A.; Ein-Mozaffari, F.; Lohi, A.; Pakzad, L. A new perspective in the evaluation of the mixing of biopolymer solutions with different coaxial mixers comprising of two dispersing impellers and a wall scraping anchor. *Chem. Eng. Res. Des.* **2016**, *114*, 202–219. [CrossRef]
65. Kazemzadeh, A.; Ein-Mozaffari, F.; Lohi, A.; Pakzad, L. Intensification of mixing of shear-thinning fluids possessing yield stress with the coaxial mixers composed of two different central impellers and an anchor. *Chem. Eng. Process. Process Intensif.* **2017**, *111*, 101–114. [CrossRef]
66. Vadlakonda, B.; Mangadoddy, N. Hydrodynamic study of three-phase flow in column flotation using electrical resistance tomography coupled with pressure transducers. *Sep. Purif. Technol.* **2018**, *203*, 274–288. [CrossRef]
67. Windows-Yule, C.R.K.; Hart-Villamil, R.; Ridout, T.; Kokalova, T.; Nogueira-Filho, C.J. Positron Emission Particle Tracking for Liquid-Solid Mixing in Stirred Tanks. *Chem. Eng. Tech.* **2020**. [CrossRef]

68. Lassaigne, M.M.; Bruno Blais, B.; Fradette, L.; Bertrand, F. Experimental investigation of the mixing of viscous liquids and non-dilute concentrations of particles in a stirred tank. *Chem. Eng. Res. Des.* **2016**, *108*, 55–68. [CrossRef]
69. Bonga, Y.E.; Eshtiaghia, N.; Wub, J.; Parthasarathy, R. Optimum solids concentration for solids suspension and solid–liquid mass transfer in agitated vessels. *Chem. Eng. Res. Des.* **2015**, *100*, 148–156. [CrossRef]
70. Grenville, R.K.; Giacomelli, J.J.; Brown, D.A.R. Suspension of solid particles in vessels agitated by Rushton turbine impellers. *Chem. Eng. Res. Des.* **2016**, *109*, 730–733. [CrossRef]
71. Wood, T.; Simmons, M.; Greenwood, J.H.; Hugh, R.W.; Stitt, E. Concentrated Slurry Formation via Drawdown and Incorporation of Wettable Solids in a Mechanically Agitated Vessel. *AIChE J.* **2018**, *64*, 1885–1895. [CrossRef]
72. Cooke, M.; Heggs, J.P.; Rodgers, T.L. The effect of solids on the dense phase gas fraction and gas–liquid mass transfer at conditions close to the heterogeneous regime in a mechanically agitated vessel. *Chem. Eng. Res. Des.* **2008**, *86*, 869–882. [CrossRef]
73. Wang, S.; Boger, D.V.; Wu, J. Energy efficient solids suspension in an agitated vessel–water slurry. *Chem. Eng. Sci.* **2012**, *74*, 233–243. [CrossRef]
74. Major-Godlewska, M.; Karcz, J. Process characteristics for gas-liquid system agitated in a vessel equipped with a turbine impeller and tubular baffles. *Chem. Pap.* **2011**, *65*, 132–138. [CrossRef]
75. Scargiali, F.; D'Orazio, A.; Grisafi, F.; Brucato, A. Modelling and simulation of gas-liquid hydrodynamics in mechanically stirred tanks. *Chem. Eng. Res. Des.* **2007**, *85*, 637–646. [CrossRef]
76. Adamiak, R.; Karcz, J. Effects of type and number of impellers and liquid viscosity on the power characteristics of mechanically agitated gas-liquid systems. *Chem. Pap.* **2007**, *61*, 16–23. [CrossRef]
77. Yianatos, J.; Contreras, F.; Diaz, F. Gas hold-up and RTD measurement in an industrial flotation cell. *Miner. Eng.* **2010**, *23*, 125–130. [CrossRef]
78. Cudak, M. Hydrodynamic characteristics of mechanically agitated air - aqueous sucrose solutions. *Chem. Process Eng.* **2014**, *35*, 97–107. [CrossRef]
79. Cudak, M.; Kiełbus-Rąpała, A.; Major-Godlewska, M.; Karcz, J. Influence of different factors on momentum transfer in mechanically agitated multiphase systems. *Chem. Proc. Eng.* **2016**, *37*, 41–53. [CrossRef]
80. Khalili, F.; Jafari Nasr, M.R.; Kazemzadeh, A.; Ein-Mozaffari, F. Hydrodynamic performance of the ASI impeller in an aerated bioreactor containing the biopolymer solution through tomography and CFD. *Chem. Eng. Res. Des.* **2017**, *125*, 190–203. [CrossRef]
81. Babaei, R.; Bonakdarpour, B.; Ein-Mozaffari, F. Analysis of gas-phase characteristics and mixing performance in an activated sludge bioreactor using electrical resistance tomography. *Chem. Eng. J.* **2015**, *279*, 874–884. [CrossRef]
82. Babaei, R.; Bonakdarpour, B.; Ein-Mozaffari, F. The use of electrical resistance tomography for the characterization of gas holdup inside a bubble column bioreactor containing activated sludge. *Chem. Eng. J.* **2015**, *268*, 260–269. [CrossRef]
83. Kazemzadeh, A.; Elias, C.; Tamer, M.; Ein-Mozaffari, F. Hydrodynamic performance of a single-use aerated stirred bioreactor in animal cell culture: Applications of tomography, dynamic gas disengagement (DGD), and CFD. *Bioprocess Biosyst. Eng.* **2018**, *41*, 679–695. [CrossRef]
84. Hashemi, N.; Ein-Mozaffari, F.; Upreti, S.R.; Hwang, D.K. Analysis of mixing in an aerated reactor equipped with the coaxial mixer through electrical resistance tomography and response surface method. *Chem. Eng. Res. Des.* **2016**, *109*, 734–752. [CrossRef]
85. Hashemi, N.; Ein-Mozaffari, F.; Upreti, S.R.; Hwang, D.K. Experimental investigation of the bubble behavior in an aerated coaxial mixing vessel through electrical resistance tomography (ERT). *Chem. Eng. J.* **2016**, *289*, 402–412. [CrossRef]
86. Sardeshpande, V.M.; Suraj Gupta, S.; Ranade, V.V. Electrical resistance tomography for gas holdup in a gas-liquid stirred tank reactor. *Chem. Eng. Sci.* **2017**, *170*, 476–490. [CrossRef]
87. Pakzad, L.; Ein-Mozaffari, F.; Chan, F. Using electrical resistance tomography and computational fluid dynamics modeling to study the formation of cavern in the mixing of pseudoplastic fluids possessing yield stress. *Chem. Eng. Sci.* **2008**, *63*, 2508–2522. [CrossRef]
88. Perumala, S.V.; Jayantib, S.; Nagarajana, K. Effect of impeller type and density difference on the draw down of low density microspheres. *Chem. Eng. Res. Design* **2015**, *104*, 571–578. [CrossRef]

89. Mahdavi, I.; Janamiri, R.; Sinkakarimi, A.; Safdari, M.; Sedaghat, M.H.; Zamani, A.; Hoseini, A.; Karimi, M. Interface Location in Single Phase Stirred Tanks. *Int. J. Chem. Mol. Eng.* **2013**, *7*, 6.
90. Ramajo, D.; Corzo, S.; Nigro, N.A. Coupled Model for Two-Phase Simulation of a Heavy Water Pressure Vessel Reactor. *Int. J. Phys. Math. Sci.* **2015**, *9*, 11.
91. Perwitasari, D.S.; Edahwati, L.; Sutiyono, S.; Karaman, N.; Jamari, J.; Muryanto, S.; Bayuseno, P.A. Effect of calcium additive on the crystallization of struvite. In *MATEC Web of Conferences, Proceedings of the 3rd Bali International Seminar on Science and Technology (BISSTECH2015), Bali, Indonesia, 15–17 October 2015*; EDP Science: Strasbourg, France, 2016; Volume 58, p. 01007.
92. Fitzpatrick, J.J.; Gloanec, F.; Michael, E. Insights from Mathematical Modelling into Process Control of Oxygen Transfer in Batch Stirred Tank Bioreactors for Reducing Energy Requirement. *Chem. Eng.* **2020**, *4*, 34. [CrossRef]
93. Szczerkowska, S.; Wiertel-Pochopien, A.; Zawala, J.; Larsenc, E.; Kowalczuk, B.P. Kinetics of froth flotation of naturally hydrophobic solids with different shapes. *Miner. Eng.* **2018**, *121*, 90–99. [CrossRef]
94. Šulc, R.; Ditl, P. The effect of process conditions on the flocculation process occurring in an agitated vessel. *Polish J. Chem. Tech.* **2012**, *14*, 88–96. [CrossRef]
95. Kasat, R.G.; Pandit, B.A. Review on Mixing Characteristics in Solid-Liquid and Solid-Liquid-Gas Reactor Vessels. *Can. J. Chem. Eng.* **2005**, *83*, 618–643.
96. Abdel-Aziz, M.H. Solid–liquid mass transfer in relation to diffusion controlled corrosion at the outer surface of helical coils immersed in agitated vessels. *Chem. Eng. Res. Design* **2013**, *91*, 43–50. [CrossRef]
97. Sedahmed, G.H.; Abdo, M.S.; Kamal, M.A.; Fadaly, O.A.; Osman, H.M. A mass transfer study of the electropolishing of metals in mechanically agitated vessels. *Int. Com. Heat Mass Transf.* **2001**, *28*, 257–265. [CrossRef]
98. Petrícek, R.; Moucha, T.; Kracíka, T.; Haidl, J. Power consumption prediction in a coalescent liquid in mechanically agitated gas–liquid reactors. *Chem. Eng. Res. Design* **2019**, *147*, 644–647.
99. Petrícek, R.; Moucha, T.; Rejl, J.F.; Valenz, L.; Haidl, J. Volumetric mass transfer coefficient in the fermenter agitated by Rushton turbines of various diameters in viscous batch. *Int. J. Heat Mass Trans.* **2017**, *115*, 856–866.
100. Petrícek, R.; Moucha, T.; Kracíka, T.; Rejl, J.F.; Valenz, L.; Haidl, J. Volumetric mass transfer coefficient in the fermenter agitated by Rushton turbines of various diameters in coalescent batch. *Int. J. Heat Mass Trans.* **2019**, *130*, 968–977.
101. Petrícek, R.; Moucha, T.; Rejl, J.F.; Valenz, L.; Haidl, J.; Cmelíková, T. Volumetric mass transfer coefficient, power input and gas hold-up in viscous liquid in mechanically agitated fermenters. Measurements and scale-up. *Int. J. Heat Mass Trans.* **2018**, *124*, 1117–1135.
102. Petrícek, R.; Moucha, T.; Rejl, J.F.; Valenz, L.; Haidl, J.; Cmelíková, T. Gas-liquid-solid volumetric mass transfer coefficient and impeller power consumptions for industrial vessel design. *Int. J. Heat Mass Trans.* **2018**, *121*, 653–662.
103. Labík, L.; Moucha, T.; Petrícek, R.; Rejl, J.F.; Valenz, L.; Haidl, J. Volumetric mass transfer coefficient in viscous liquid in mechanically agitated fermenters. Measurement and correlation. *Chem. Eng. Sci.* **2017**, *170*, 451–463. [CrossRef]
104. Loubière, C.; Delafosse, A.; Guedon, E.; Chevalot, I.; Toye, D.; Olmos, E. Dimensional analysis and CFD simulations of microcarrier 'just-suspended' state in mesenchymal stromal cells bioreactors. *Chem. Eng. Sci.* **2019**, *203*, 464–474. [CrossRef]
105. Drewer, G.R.; Ahmed, N.; Jameson, G.J. An Optimum Concentration for the Suspension of Solids in Stirred Vessels. In *Mixing and Crystallization*; Academic Publishers: Kluwer, The Netherlands, 2000.
106. Kasat, G.R.; Khopkar, A.R.; Ranade, V.V.; Pandit, A.B. CFD simulation of liquid-phase mixing in solid-liquid stirred reactor. *Chem. Eng. Sci.* **2008**, *63*, 3877–3885. [CrossRef]
107. Wu, J.; Nguyen, B.; Graham, L. Mixing Intensification for the Mineral Industry. *Can. J. Chem. Eng.* **2010**, *88*, 447–454. [CrossRef]
108. Wang, S.; Parthasarathy, R.; Bong, Y.E.; Wu, J.; Slatter, P. Suspension of Ultrahigh Concentration Solids in an Agitated Vessel. *AIChE J.* **2012**, *58*, 1291–1302. [CrossRef]
109. Cudak, M.; Karcz, J.; Major-Godlewska, M. *Problems of Heat Transfer in Agitated Vessels. In Practical Aspects of Chemical Engineering*; Springer: Cham, Switzerland, 2018; pp. 35–50.

110. Suchecki, W. Investigation of the sedimentation process using flow visualization methods. *Chem. Proc. Eng.* **2019**, *40*, 223–233.
111. Tamburini, A.; Cipollina, A.; Micale, G.; Brucato, A. Particle distribution in dilute solid liquid unbaffled tanks via a novel laser sheet and image analysis based technique. *Chem. Eng. Sci.* **2013**, *87*, 341–358. [CrossRef]
112. Zheng, Y.; Zhang, Q. Simultaneous measurement of gas and solid holdups in multiphase systems using ultrasonic technique. *Chem. Eng. Sci.* **2004**, *59*, 3505–3514. [CrossRef]
113. Chang, J.S.; Ichikawa, Y.; Irons, G.A.; Morala, E.C.; Wan, P.T. Void fraction measurement by an ultrasonic transmission technique in bubbly gas–liquid two-phase flow. In *Measuring Techniques in Gas–Liquid Two-Phase Flows*; Delhaye, J.M., Cognet, G., Eds.; Springer: New York, NY, USA, 1984.
114. Bałyga, J.; Jasińska, M. Energetic Efficiency of Mixing and Mass Transfer in Single Phase and Two-Phase Systems. *Chem. Proc. Eng.* **2017**, *38*, 79–96. [CrossRef]
115. Khalili, F.; JafariNasr, M.R.; Kazemzadeh, A.; Ein-Mozaffari, F. Analysis of gas holdup and bubble behavior in a biopolymer solution inside a bioreactor using tomography and dynamic gas disengagement techniques. *J. Chem. Technol. Biotechnol.* **2018**, *93*, 340–349. [CrossRef]
116. Kazemzadeh, A.; Ein-Mozaffari, F.; Lohi, A. Mixing of highly concentrated slurries of large particles: Applications of electrical resistance tomography (ERT) and response surface methodology (RSM). *Chem. Eng. Res. Des.* **2019**, *143*, 226–240. [CrossRef]
117. Patel, D.; Ein-Mozaffari, F.; Mehrvar, M. Using Tomography to Characterize the Mixing of Non-Newtonian Fluids with a Maxblend Impeller. *Chem. Eng. Tech.* **2013**, *36*, 687–695. [CrossRef]
118. Mishra, P.; Ein-Mozaffari, F. Critical review of different aspects of liquid-solid mixing operations. *Rev. Chem. Eng.* **2020**, *36*, 555–592. [CrossRef]
119. Vinnett, Z.; Contreras, F.; Yianatos, J. Gas dispersion pattern in mechanical flotation cells. *Miner. Eng.* **2012**, *26*, 80–85. [CrossRef]
120. Yianatos, J.B. Fluid flow and kinetic modelling in flotation related processes Columns and Mechanically Agitated Cells—A Review. *Trans. IChemE Part A Chem. Eng. Res. Des.* **2007**, *85*, 1591–1603. [CrossRef]
121. Trahar, W.J.; Warren, L.J. The flotability of very fine particles—A review. *Int. J. Miner. Process.* **1976**, *3*, 103–131. [CrossRef]
122. Brożek, M.; Młynarczykowska, A. Probability of detachment of particle determined according to the stochastic model of flotation kinetics. *Physicochem. Probl. Min. Process.* **2010**, *44*, 23–34.
123. Brożek, M.; Młynarczykowska, A. The relation between the dispersive model of the particle and the distribution of permanent adhesion rate constant in the coal flotation process. *Min. Res. Manag.* **2008**, *24*, 63–82.
124. Koh, P.T.L.; Manickam, M.; Schwarz, M.P. CFD simulation of bubble-particle collisions in mineral flotation cells. *Miner. Eng.* **2000**, *13*, 1455–1463. [CrossRef]
125. Saramak, D.; Krawczykowska, A.; Młynarczykowska, A. Effects of high pressure ore grinding on the efficiency of flotation operations. *Arch. Min. Sci.* **2014**, *59*, 731–740. [CrossRef]
126. Brożek, M.; Młynarczykowska, A. Application of the stochastic model for analysis of flotation kinetics with coal as an example. *Physicochem. Probl. Miner. Process.* **2006**, *40*, 31–44.
127. Finch, J.A.; Dobby, G.S. *Column Flotation*, 1st ed.; Pergamon Press: London, UK, 1990.
128. Brożek, M.; Młynarczykowska, A. The distribution of air bubble size in the pneumo-mechanical flotation machine. *Arch. Min. Sci.* **2012**, *57*, 729–740.
129. Młynarczykowska, A.; Nyrek, A.; Oleksik, K. Analysis of the gas phase in flotation process. Experimental determination of the volume of air bubbles in the pneumo-mechanical flotation machine. *J. Pol. Min. Eng. Soc.* **2015**, *16*, 181–188.
130. Młynarczykowska, A.; Oleksik, K. Analysis of the gas phase in flotation process. Pt. 2, Empirical functions of occurrence frequency of tested parameters. *J. Pol. Min. Eng. Soc.* **2017**, *18*, 257–262.
131. Busciglio, A.; Grisafi, F.; Scargiali, F.; Brucato, A. On the measurement of local gas hold-up, interfacial area and bubble size distribution in gas–liquid contactors via light sheet and image analysis: Imaging technique and experimental results. *Chem. Eng. Sci.* **2013**, *102*, 551–566. [CrossRef]
132. Pal, R.; Masliyah, J. Flow characteristics of a flotation column. *Can. J. Chem. Eng.* **1990**, *29*, 97–103.
133. Xu, M.; Finch, J.A.; Uribe-Salas, A. Maximum gas and bubble surface rates in flotation columns. *Int. J. Miner. Process.* **1991**, *32*, 233–250. [CrossRef]

134. Langberg, D.E.; Jameson, G.J. The coexistence of the froth and liquid phases in a flotation column. *Chem. Eng. Sci.* **1999**, *247*, 4345–4355. [CrossRef]
135. Brożek, M.; Młynarczykowska, A. Analysis of kinetics models of batch flotation. *Physicochem. Probl. Min. Process.* **2007**, *41*, 51–65.
136. Basavarajappa, M.; Miskovic, S. Investigation of gas dispersion characteristics in stirred tank and flotation cell using a corrected CFD-PBM quadrature-based moment method approach. *Miner. Eng.* **2016**, *95*, 161–184. [CrossRef]
137. Yianatos, J.B.; Henríquez, F. Boundary conditions for gas rate and bubble size at the pulp-froth interface in flotation equipment. *Miner. Eng.* **2007**, *20*, 625–628. [CrossRef]
138. Pyke, B.; Duan, J.; Fornasiero, D.; Ralston, J. From turbulence and collision to attachment and detachment: A general flotation model. In *Fundamentals to Applications, Proceedings of the Strategic Conference Flotation and Flocculation, Kailua-Kona, Hawaii, 28 July–2 August 2002*; Ralston, J., Miller, J., Rubio, J., Eds.; Snap Printing: Adelaide, Australia, 2003; pp. 77–89.
139. Koh, P.T.L.; Schwarz, M.P. CFD modelling of bubble–particle attachments in flotation cells. *Miner. Eng.* **2006**, *19*, 619–626. [CrossRef]
140. Bloom, F.; Heindel, T.J. On the structure of collision and detachment frequencies in flotation models. *Chem. Eng. Sci.* **2002**, *57*, 2467–2473. [CrossRef]
141. Musiał, M.; Karcz, J.; Cudak, M. Numerical analysis of momentum transfer processes in a mechanically agitated Air—Biophase—Liquid system. *Chem. Proc. Eng.* **2017**, *38*, 465–475. [CrossRef]
142. Koh, P.T.L.; Schwarz, M.P. CFD modeling of bubble particle collision rates and efficiencies in a flotation cell. *Miner. Eng.* **2003**, *16*, 1055–1059. [CrossRef]
143. Jaszczur, M.; Młynarczykowska, A.; Hanus, R. An analysis of the velocity field distribution inside the flotation chamber. *J. Phys. Conf. Ser.* **2016**, *745*, 032121. [CrossRef]
144. Finch, J.A. Column flotation: A selected review—Part IV: Novel flotation devices. *Miner. Eng.* **1995**, *8*, 587–602. [CrossRef]
145. Evansa, G.M.; Doroodchia, E.; Laneb, G.L.; Koh, P.T.L.; Schwarz, M.P. Mixing and gas dispersion in mineral flotation cells. *Chem. Eng. Res. Des.* **2008**, *86*, 1350–1362. [CrossRef]
146. Deglon, D.A.; Meyer, C.J. CFD modelling of stirred tanks: Numerical considerations. *Miner. Eng.* **2006**, *19*, 1059–1068. [CrossRef]
147. Lane, G.L.; Schwarz, M.P.; Evans, G.M. Numerical modeling of gas–liquid flow in stirred tanks. *Chem. Eng. Sci.* **2005**, *60*, 2203–2214. [CrossRef]
148. Smith, J.M. Dispersion of gases in liquids: The hydrodynamics of gas dispersion in low viscosity liquids. In *Mixing of Liquids by Mechanical Agitation*; Ulbrecht, J.J., Patterson, G.K., Eds.; Gordon and Breach: New York, NY, USA, 1985; pp. 139–201.
149. Cooke, M.; Heggs, P.J.; Eaglesham, A.; Housley, D. Bubble studies under cold and boiling conditions using dynamic gas disengagement coupled with video and photographic techniques. In Proceedings of the Eurotherm, 12th International Heat Transfer Conference, Grenoble, France, 18–23 August 2002; Volume 71, pp. 95–101.
150. Ozcan, O.; Calimli, A.; Berber, B.; Oguz, H. Effect of inert solid particles at low concentrations on gas–liquid mass transfer in mechanically agitated tanks. *Chem. Eng. Sci.* **2000**, *55*, 2737–2740. [CrossRef]
151. Gentile, F.; Oleschko, H.; Veverka, P.; Machon, V.; Paglainti, A.; Bujalski, W.; Etchells, A.W.; Nienow, A.W. Some effects of particle wettability in agitated solid–gas–liquid systems: Gas–liquid mass transfer and the dispersion of floating solids. *Can. J. Chem. Eng.* **2003**, *81*, 581–587. [CrossRef]
152. Davoody, M.; Raman, A.A.B.A.; Parthasarathy, R. Chemical, Maximizing gas–liquid interfacial area in a three-phase stirred vessel operating at high solids concentrations. *Eng. Process.* **2016**, *104*, 133–147. [CrossRef]
153. Scargiali, F.; Busciglio, A.; Grisafi, F.; Brucato, A. Gas–liquid–solid operation of a high aspect ratio self-ingesting reactor. *Int. J. Chem. Reactor Eng.* **2012**, *10*, A27. [CrossRef]
154. Madhania, S.; Nurtono, T.; Winardi, S.; Muharam, Y.; Purwanto, W.W. Computational study of the time-dependent flow field of a water-molasses mixture inside a stirred vessel. *Int. J. Technol.* **2019**, *10*, 561–570. [CrossRef]
155. Wu, B. CFD Investigation of Turbulence Models for Mechanical Agitation of Non-Newtonian Fluids in Anaerobic Digesters. *Water Res.* **2011**, *45*, 2082–2094. [PubMed]

156. Kamil, M.; Bushra, A.; Ahmad, A. Minimum agitation speed for liquid–liquid–gas dispersion in mechanically agitated vessels. *Chem. Eng. Process.* **2001**, *40*, 49–57. [CrossRef]
157. Skelland, P.H.A.; Ramsey, G.G. Minimum agitator speed for complete liquid-liquid dispersion. *Ind. Eng. Chem. Res.* **1987**, *26*, 77–81. [CrossRef]
158. Madhania, S.; Cahyani, A.B.; Nurtono, T.; Muharam, Y.; Winardi, S.; Purwanto, W.W. CFD Study of Mixing Miscible Liquid with High Viscosity Difference in a Stirred Tank. In *IOP Conference Series: Materials Science and Engineering, Proceedings of the International Symposium on Materials, Metallurgy, and Chemical Engineering, Bali, Indonesia, 24–27 July 2017*; IOP Publishing Ltd.: Bristol, England, 2018; Volume 316.
159. Madhania, S.; Nurtono, T.; Cahyani, A.B.; Muharam, Y.; Winardi, S.; Purwanto, W.W. Mixing Behaviour of Miscible Liquid-liquid Multiphase Flow in Stirred Tank with Different Marine Propeller Installment by Computational Fluid Dynamics Method. *Chem. Eng. Trans.* **2017**, *56*, 1057–1062.
160. Suekuni, M.T.; Myers, T.R.; McNeil, M.C.; Prisco, A.J.; Shelburne, S.S.; Shepperson, W.A.; Allgeier, A.M. Surface Area Determination of Kevlar® Particles in Suspensions Containing Iron Impurities Using Low-Field Nuclear Magnetic Resonance Relaxometry. *ACS Appl. Polym. Mater.* **2020**, *2*, 2134–2141. [CrossRef]
161. Wöckel, S.; Hempel, U.; Auge, J. Acousto-capacitive tomography of liquid multiphase systems. *Sens. Actuators A Phys.* **2011**, *172*, 322–329. [CrossRef]
162. Li, L.C.; Chen, N.; Xiang, K.F.; Xiang, B.P. A Comparative CFD Study on Laminar and Turbulent Flow Fields in Dual-Rushton Turbine Stirred Vessels. *J. App. Fluid Mech.* **2020**, *13*, 413–427. [CrossRef]
163. Farzan, P.; Ierapetritou, M.G. Integrated modeling to capture the interaction of physiology and fluid dynamics in biopharmaceutical bioreactors. *Comp. Chem. Eng.* **2017**, *97*, 271–282. [CrossRef]
164. Liang, Y.N.; Gao, D.R.; Bai, L. Numerical simulation of the laminar flow field and mixing time in stirred tank with double layer impeller. *Chin. J. Mech. Eng.* **2015**, *51*, 185–195. [CrossRef]
165. Cokljat, D.; Slack, M.; Vasquez, S.A.; Bakker, A.; Montante, G. Reynolds-Stress Model for Eulerian Multiphase. *Prog. Comp. Fluid Dyn.* **2006**, *6*, 168–178. [CrossRef]
166. Zalc, J.M.; Szalai, E.S.; Alvarez, M.M.; Muzzio, F.J. Using CFD to understand chaotic mixing in laminar stirred tanks. *AIChE J.* **2002**, *48*, 2124–2134. [CrossRef]
167. Bezzo, F.; Macchietto, S.; Pantelides, C.C. A general methodology for hybrid multizonal/CFD models. *Comput. Chem. Eng.* **2004**, *28*, 501–511. [CrossRef]
168. Márquez-Baños, E.V.; Concha-Gómez, D.A.; Valencia-López, J.J.; López-Yáñez, A.; Ramírez-Muñoz, J. Shear rate and direct numerical calculation of the Metzner-Otto constant for a pitched blade turbine. *J. Food Eng.* **2019**, *257*, 10–18.
169. Pakzad, L.; Ein-Mozaffari, F.; Upreti, R.S.; Lohi, A. Experimental and numerical studies on mixing of yield-pseudoplastic fluids with a coaxial mixer. *Chem. Eng. Comm.* **2013**, *200*, 1553–1577. [CrossRef]
170. Ameur, H. Modifications in the Rushton turbine for mixing viscoplastic fluids. *J. Food Eng.* **2018**, *233*, 117–125. [CrossRef]
171. Tamburini, A.; Gagliano, G.; Micale, G.; Brucato, A.; Scargiali, F.; Ciofalo, M. Direct numerical simulation of creeping to early turbulent flow in unbaffled and baffled stirred tanks. *Chem. Eng. Sci.* **2018**, *192*, 161–175. [CrossRef]
172. Ramírez-Muñoz, J.; Guadarrama-Pérez, R.; Márquez-Baños, V.E. A direct calculation method of the Metzner-Otto constant by using computational fluid dynamics. *Chem. Eng. Sci.* **2017**, *174*, 347–353. [CrossRef]
173. Ramírez-Muñoz, J.; Martínez-de-Jesús, G.; Soria, A.; Alonso, A.; Torres, L.G. Assessment of the effective viscous dissipation for deagglomeration processes induced by a high shear impeller in a stirred tank. *Powder Technol.* **2016**, *27*, 1885–1897. [CrossRef]
174. Fathi, R.S.; Turcotte, G.; Dhib, R.; Ein, M.F. CFD modelling of the mixing of water in oil emulsions. *Comp. Chem. Eng.* **2012**, *45*, 124–136. [CrossRef]
175. Chtourou, W.; Ammar, M.; Driss, Z.; Abid, M.S. CFD Prediction of the turbulent flow generated in a stirred square tank by a Rushton turbine. *Energy Power Eng.* **2014**, *6*, 95. [CrossRef]
176. Joshi, J.B.; Nere, N.K.; Rane, C.V.; Murthy, B.N.; Mathpati, C.S.; Patwardhan, A.W.; Ranade, V.V. Comparison of turbulence models. Part I: Radial flow impellers. *Can. J. Chem. Eng.* **2011**, *89*, 23–82. [CrossRef]
177. Joshi, J.B.; Nere, N.K.; Rane, C.V.; Murthy, B.N.; Mathpati, C.S.; Patwardhan, A.W.; Ranade, V.V. CFD simulation of stirred tanks: Comparison of turbulence models (Part II: Axial flow impellers, multiple impellers and multiphase dispersions). *Can. J. Chem. Eng.* **2011**, *89*, 754–816. [CrossRef]

178. Wang, C.-Y.; Gu, J.-J.; Feng, X.-P.; Ge, L.-F. CFD simulation and PIV measurement of the flow field generated by modified pitched blade turbine impellers. *Chem. Eng. Res. Des.* **2014**, *92*, 1027–1036.
179. Lin, A.; Sun, Y.; Zhang, H.; Lin, X.; Yang, L.; Zheng, Q. Fluctuating characteristics of air-mist mixture flow with conjugate wall-film motion in a compressor of gas turbine. *App. Therm. Energy* **2018**, *142*, 779–792. [CrossRef]
180. Delafosse, A.; Loubière, C.; Calvo, S.; Toye, D.; Olmos, E. Solid-liquid suspension of microcarriers in stirred tank bioreactor-experimental and numerical analysis. *Chem. Eng. Sci.* **2018**, *180*, 52–63. [CrossRef]
181. Placek, J.; Tavlarides, L.L.; Smith, G.W.; Fort, I. Turbulent flow in stirred tanks. II. A two-scale model of turbulence. *AIChE J.* **1986**, *31*, 1113–1120. [CrossRef]
182. Pericleous, K.A.; Patel, M. The modelling of tangential and axial agitators in chemical reactors. *Physicochem. Hydrodyn.* **1987**, *8*, 105–123.
183. Ranade, V.V.; Joshi, J.B.; Marathe, A.G. Flow generated by pitched blade turbines. II. Simulation using k-ε model. *Chem. Eng. Commun.* **1989**, *81*, 225–248. [CrossRef]
184. Kresta, S.M.; Wood, P.E. Prediction of the three-dimensional flow in stirred tanks. *Am. Inst. Chem. Eng. J.* **1991**, *37*, 448–460. [CrossRef]
185. Ramírez-Gómez, R.; García-Cortés, D.; Martínez-de Jesús, G.; González-Brambila, M.M.; Alonso, A.; Martínez-Delgadillo, S.A.; Ramírez Muñoz, J. Performance Evaluation of Two High-Shear Impellers in an Unbaffled Stirred Tank. *Chem. Eng. Technol.* **2015**, *38*, 1519–1529. [CrossRef]
186. Zalc, J.M.; Alvarez, M.M.; Muzzio, F.J.; Arik, B.E. Extensive validation of computed laminar flow in a stirred tank with three Rushton turbines. *AIChE J.* **2001**, *47*, 2144–2154. [CrossRef]
187. Pakzad, L.; Ein-Mozaffari, F.; Upreti, S.R.; Lohi, A. Characterisation of the mixing of non-newtonian fluids with a scaba 6SRGT impeller through ert and CFD. *Can. J. Chem. Eng.* **2013**, *91*, 90–100. [CrossRef]
188. Kelly, W.; Gigas, B. Using CFD to predict the behaviour of power law fluids near axial-flow impellers operating in the transitional flow regime. *Chem. Eng. Sci.* **2003**, *58*, 2141–2152. [CrossRef]
189. Ranade, V.V.; Shashidhar, S.; Karve, H.R. A computational study of gas accumulation and cavity formation behind blades: Influence of blade shapes. In Proceedings of the International Conference on Multiphase Flows, New Orleans, LA, USA, 27 May–1 June 2001; Elsevier Publisher: Amsterdam, The Netherlands, 2002.
190. Khopkar, A.R.; Kasat, G.R.; Pandit, A.B.; Ranade, V.V. CFD simulation of mixing in tall gas–liquid stirred vessel: Role of local flow patterns. *Chem. Eng. Sci.* **2006**, *61*, 2912–2929. [CrossRef]
191. Khopkar, A.R.; Ranade, V.V. CFD simulation of gas–liquid stirred vessel: VC, S33, and L33 flow regimes. *AIChE J.* **2006**, *52*, 1654–1672. [CrossRef]
192. Morud, K.E.; Hjertager, B.H. LDA measurements and CFD modeling of gas–liquid flow in a stirred vessel. *Chem. Eng. Sci.* **1996**, *51*, 233–249. [CrossRef]
193. Pinelli, D. A phenomenological model for the gas phase flow in high-aspect-ratio stirred vessels: The role of small bubbles in non-coalescent and moderately viscous liquids. *Chem. Eng. Sci.* **2005**, *60*, 2239–2252. [CrossRef]
194. Deen, N.G.; Solberg, T.; Hjertager, H.B. Flow generated by an aerated Rushton impeller: Two-phase PIV experiments and numerical simulations. *Can. J. Chem. Eng.* **2002**, *80*, 1–15. [CrossRef]
195. Sun, H.Y.; Mao, Z.S.; Yu, G.Z. Experimental and numerical study of gas hold-up in surface aerated stirred tanks. *Chem. Eng. Sci.* **2006**, *61*, 4098–4110. [CrossRef]
196. Khopkar, A.R.; Tanguy, P.A. CFD simulation of gas–liquid flows in stirred vessel equipped with dual Rushton turbines: Influence of parallel, merging and diverging flow configurations. *Chem. Eng. Sci.* **2008**, *63*, 3810–3820. [CrossRef]
197. Venneker, B.C.H.; Derksen, J.J.; Van Den Akker, H.E.A. Population balance modeling of aerated stirred vessels based on CFD. *AIChE J.* **2002**, *48*, 673–684. [CrossRef]
198. Torré, J.P.; Fletcher, D.F.; Lasuye, T.; Xuereb, C. Single and multiphase CFD approaches for modelling partially baffled stirred vessels comparison of experimental data with numerical predictions. *Chem. Eng. Sci.* **2007**, *62*, 6246–6262. [CrossRef]
199. Jahoda, M.; Tomaskova, L.; Mostek, M. CFD prediction of liquid homogenization in a gas–liquid stirred tank. *Chem. Eng. Res. Des.* **2009**, *87*, 460–467. [CrossRef]
200. Wang, H.; Xiaoqiang, J.; Wang, X.; Zhou, Z.; Wen, J.; Zhang, J. CFD modeling of hydrodynamic characteristics of a gas–liquid two-phase stirred tank. *App. Math. Model.* **2014**, *38*, 63–92. [CrossRef]

201. Khopkar, A.R.; Kasat, G.R.; Pandit, A.B.; Ranade, V.V. Computational Fluid Dynamics Simulation of the Solid Suspension in a Stirred Slurry Reactor. *Ind. Eng. Chem. Res.* **2006**, *45*, 4416–4428. [CrossRef]
202. Li, X.; Guan, X.; Rongtao, Z.R.; Yang, N.; Liu, M. CFD Simulation of Gas Dispersion in a Stirred Tank of Dual Rushton Turbines. *Int. J. Chem. Reactor Eng.* **2017**, *15*, 4. [CrossRef]
203. Zhang, Y.H.; Yong, Y.M.; Mao, Z.S.; Yang, C.; Sun, H.Y.; Wang, H.L. Numerical simulation of gas-liquid flow in a stirred tank with swirl modification. *Chem. Eng. Tech.* **2009**, *32*, 1266–1273. [CrossRef]
204. Buffo, A.; Vanni, M.; Marchisio, D.L. Multidimensional population balance model for the simulation of turbulent gas–liquid systems in stirred tank reactors. *Chem. Eng. Sci.* **2012**, *70*, 31–44. [CrossRef]
205. Lin, X.Y.; Wang, K.; Zhang, J.S.; Luo, G.S. Liquid-liquid mixing enhancement rules by microbubbles in three typical micro-mixers. *Chem. Eng. Sci.* **2015**, *127*, 60–71. [CrossRef]
206. Shi, P.; Rzehak, R. Bubbly flow in stirred tanks: Euler-Euler/RANS modeling. *Chem. Eng. Sci.* **2018**, *190*, 419–435. [CrossRef]
207. Aranowski, R.; Wojewódka, P.; Zielińska-Jurek, A.; Bokotko, R.; Jungnickel, C. Spinning Fluids Reactor: A new design of a gas-liquid contactor. *Chem. Eng. Proc. Process Intensif.* **2017**, *116*, 40–47. [CrossRef]
208. Hsu, R.C.; Chiu, C.K.; Lin, S.C. A CFD study of the drawdown speed of floating solids in a stirred vessel. *J. Taiwan Inst. Chem. Eng.* **2018**, *90*, 33–43. [CrossRef]
209. Liao, Y.; Rzehak, R.; Lucas, D.; Krepper, E. Baseline closure model for dispersed bubbly flow: Bubble coalescence and breakup. *Chem. Eng. Sci.* **2015**, *122*, 336–349. [CrossRef]
210. Murthy, B.N.; Ghadge, R.S.; Joshi, J.B. CFD simulations of gas–liquid–solid stirred reactor: Prediction of critical impeller speed for solid suspension. *Chem. Eng. Sci.* **2007**, *62*, 7184–7195. [CrossRef]
211. Jia, X.; Wen, J.; Feng, W.; Yuan, Q. Local hydrodynamics modeling of a gas-liquid-solid three-phase airlift loop reactor. *Ind. Eng. Chem. Res.* **2007**, *46*, 5210–5220. [CrossRef]
212. Gakingo, G.K.; Clarke, K.G.; Louw, T.M. A numerical investigation of the hydrodynamics and mass transfer in a three-phase gas-liquid-liquid stirred tank reactor. *Biochem. Eng. J.* **2020**, *157*, 107522. [CrossRef]
213. Fogler, H.S. *Essentials of Chemical Reaction Engineering*; Pearson Education: Upper Saddle River, NJ, USA, 2010.
214. Cheng, D.; Feng, X.; Cheng, J.C.; Yang, C. Numerical simulation of macro-mixing in liquid-liquid stirred tanks. *Chem. Eng. Sci.* **2013**, *101*, 272–282. [CrossRef]
215. Reinecke, S.F.; Deutschmann, A.; Jobst, K.; Hampel, U. Macro-mixing characterisation of a stirred model fermenter of non-Newtonian liquid by flow following sensor particles and ERT. *Chem. Eng. Res. Des.* **2017**, *118*, 1–11. [CrossRef]
216. Uebel, K.; Rößger, P.; Prüfert, U.; Richter, A.; Meyer, B. CFD-based multi-objective optimization of a quench reactor design. *Fuel Process. Technol.* **2016**, *149*, 290–304. [CrossRef]
217. Rößger, P.; Richter, A. Performance of different optimization concepts for reactive flow systems based on combined CFD and response surface methods. *Comp. Chem. Eng.* **2018**, *108*, 232–239. [CrossRef]
218. Na, J.; Kshetrimayum, K.S.; Lee, U.; Han, C. Multi-objective optimization of microchannel reactor for Fischer-Tropsch synthesis using computational fluid dynamics and genetic algorithm. *Chem. Eng. J.* **2017**, *313*, 1521–1534. [CrossRef]
219. Sierra-Pallares, J.; del Valle, J.G.; Paniagua, J.M.; Garcia, J.; Mendez-Bueno, C.; Castro, F. Shape optimization of a long-tapered R134 a ejector mixing chamber. *Energy* **2018**, *165*, 422–438. [CrossRef]
220. Brar, L.S.; Elsayed, K. Analysis and optimization of cyclone separators with eccentric vortex finders using large eddy simulation and artificial neural network. *Sep. Purif. Technol.* **2018**, *207*, 269–283. [CrossRef]
221. Park, S.; Na, J.; Kim, M.; Lee, J.M. Multi-objective Bayesian optimization of chemical reactor design using computational fluid dynamics. *Comp. Chem. Eng.* **2018**, *119*, 25–37. [CrossRef]
222. Karcz, J.; Mackiewicz, B. Effects of vessel baffling on the drawdown of floating solids. *Chem. Pap.* **2009**, *63*, 164–171. [CrossRef]
223. Khazam, O.; Kresta, S.M. A novel geometry for solids drawdown in stirred tanks. *Chem. Eng. Res. Des.* **2009**, *87*, 280–290. [CrossRef]
224. Bhosekar, A.; Ierapetritou, M. Advances in surrogate based modeling, feasibility analysis, and optimization: A review. *Comput. Chem. Eng.* **2018**, *108*, 250–267. [CrossRef]
225. Jones, D.R.; Schonlau, M.; Welch, W.J. Efficient global optimization of expensive black-box functions. *J. Glob. Optim.* **1998**, *13*, 455–492. [CrossRef]

226. Regis, R.G. Trust regions in Kriging-based optimization with expected improvement. *Eng. Optim.* **2016**, *48*, 1037–1059. [CrossRef]
227. Ding, J.; Wang, X.; Zhou, X.F.; Ren, N.Q.; Guo, W.Q. CFD optimization of continuous stirred-tank (CSTR) reactor for biohydrogen production. *Bioresour. Technol.* **2010**, *101*, 7005–7013. [CrossRef] [PubMed]
228. Priyadi, K.; Lu, C.T.; Sutanto, H. Optimization of impeller design for stirred tank using computational fluid dynamics. *IOP Conf. Ser. Mater. Sci. Eng.* **2019**, *567*, 01203. [CrossRef]
229. Wutz, J.; Waterkotte, B.; Heitmann, K.; Wucherpfennig, T. Computational fluid dynamics (CFD) as a tool for industrial UF/DF tank optimization. *Biochem. Eng. J.* **2020**, *16*, 107617. [CrossRef]
230. Yang, S.; Kiang, S.; Farzan, P.; Ierapetritou, M. Optimization of Reaction Selectivity Using CFD-Based Compartmental Modeling and Surrogate-Based Optimization. *Processes* **2018**, *7*, 9. [CrossRef]
231. Jaszczur, M.; Szmyd, J.; Petermann, M. An analysis of mixing process in a static mixer. In *Mechanics of 21st Century—ICTAM04, Proceedings of the 21st International Congress of Theoretical and Applied Mechanics, Warsaw, Poland, 15–21 August 2004*; Published by Kluwer/Springer Academic Publishers: Amsterdam, The Netherlands, 2009.
232. Sk, A.A.; Kumar, P.; Kumar, S. Experimental studies of helical coils in laminar regime for mechanically agitated vessel. *Proc. IMechE Part E J. Proc. Mech. Eng* **2020**, *234*, 173–181. [CrossRef]
233. Abdelhamid, A.S.; Armenante, M.P. Effect of Tank Bottom Shapes on N_{js} and Power Dissipation in Stirred Vessels under Different Baffling Configurations. *Chem. Proc. Eng.* **2013**, *34*, 293–307.
234. Sommerfeld, M.; Schmalfuß, S. Analysis and optimisation of particle mixing performance in fluid phase resonance mixers based on Euler/Lagrange calculations. *Adv. Pow. Technol.* **2020**, *31*, 139–157. [CrossRef]
235. Derksen, J.J. Eulerian-Lagrangian simulations of settling and agitated dense solid-liquid suspensions—Achieving grid convergence. *AIChE J.* **2018**, *64*, 1147–1158. [CrossRef]
236. Moilanen, P.; Laakkonen, M.; Visuri, O.; Aittamaa, J. Modeling local gas–liquid mass transfer in agitated viscous shear-thinning dispersions with CFD. *Ind. Eng. Chem. Res.* **2007**, *46*, 7289–7299. [CrossRef]
237. Kerdouss, F.; Bannari, A.; Proulx, P. CFD modeling of gas dispersion and bubble size in a double turbine stirred tank. *Chem. Eng. Sci.* **2006**, *61*, 3313–3322. [CrossRef]
238. Li, G.; Li, H.; Wei, G.; He, X.; Xu, S.; Chen, K.; Ouyang, P.; Ji, X. Hydrodynamics, mass transfer and cell growth characteristics in a novel microbubble stirred bioreactor employing sintered porous metal plate impeller as gas sparger. *Chem. Eng. Sci.* **2018**, *192*, 665–677. [CrossRef]
239. Rzehak, R.; Krepper, E. Euler-Euler simulation of mass-transfer in bubbly flows. *Chem. Eng. Sci.* **2016**, *155*, 459–468. [CrossRef]
240. Sommerfeld, M.; Decker, S. Modeling of gas-liquid mass transfer in a stirred tank bioreactor agitated by a Rushton turbine or a new pitched blade impeller. *Bioprocess Biosys. Eng.* **2004**, *37*, 365–375.
241. Pilarek, M.; Sobieszuk, P.; Wierzchowski, K.; Dabkowska, K. Impact of operating parameters on values of a volumetric mass transfer coefficient in a single-use bioreactor with wave-induced agitation. *Chem. Eng. Res. Des.* **2018**, *136*, 1–10. [CrossRef]
242. Ghobadi, N.; Ogino, C.; Yamabe, K.; Ohmura, N. Characterizations of the submerged fermentation of Aspergillus oryzae using a full zone impeller in a stirred tank bioreactor. *J. Biosci. Bioeng.* **2017**, *123*, 101–108. [CrossRef]
243. Gimbun, J.; Rielly, C.D.; Nagy, Z.K. Modelling of mass transfer in gas–liquid stirred tanks agitated by Rushton turbine and CD-6 impeller: A scale-up study. *Chem. Eng. Res. Des.* **2009**, *87*, 437–451. [CrossRef]
244. Laakkonen, M.; Moilanen, P.; Alopaeus, V.; Aittamaa, J. Modelling local bubble size distribution in agitated vessels. *Chem. Eng. Sci.* **2007**, *62*, 721–740. [CrossRef]
245. Laakkonen, M.; Moilanen, P.; Alopaeus, V.; Aittamaa, J. Modelling local gas–liquid mass transfer in agitated vessels. *Chem. Eng. Res. Des.* **2007**, *85*, 665–675. [CrossRef]
246. Bai, Y.; Moo-Young, M.; Anderson, A.W. Characterization of power input and its impact on mass transfer in a rocking disposable bioreactor. *Chem. Eng. Sci.* **2019**, *209*, 115–183. [CrossRef]
247. Jones, M.J.S.; Louw, M.T.; Harrison, T.L.S. Energy consumption due to mixing and mass transfer in a wave photobioreactor. *Algal Res.* **2017**, *24*, 317–324. [CrossRef]
248. Khopkar, A.R.; Mavros, P.; Ranade, V.V.; Bertrand, J. Simulation of flow generated by an axial-flow impeller: Batch and continuous operation. *Chem. Eng. Res. Des.* **2004**, *82*, 737–751. [CrossRef]
249. Li, M.; White, G.; Wilkinson, D.; Roberts, K.J. LDA measurements and CFD modelling of a stirred vessel with a retreat curve impeller. *Ind. Eng. Chem. Res.* **2004**, *43*, 6534–6547. [CrossRef]

250. Verzicco, R.; Fatica, M.; Iaccarino, G.; Orlandi, P. Flow in an impeller stirred tank using an immersed-boundary method. *AIChE J.* **2004**, *50*, 1109–1118. [CrossRef]
251. Gillissen, J.J.J.; Van den Akker, H.E. Direct Numerical Simulation of the turbulent flow in a baffled tank driven by a Rushton turbine. *AIChE J.* **2012**, *58*, 3878–3890. [CrossRef]
252. Devi, T.T.; Kumar, B.; Patel, A.K. Detached eddy simulation of turbulent flow in stirred tank reactor. *Procedia Eng.* **2015**, *127*, 87–94. [CrossRef]
253. Shu, S.; Yang, N. GPU-Accelerated Large Eddy Simulation of Stirred Tanks. *Chem. Eng. Sci.* **2018**, *181*, 132–145. [CrossRef]
254. Alcamo, R.; Micale, G.; Grisafi, F.; Brucato, A.; Ciofalo, M. Large-eddy simulation of turbulent flow in an unbaffled stirred tank driven by a Rushton turbine. *Chem. Eng. Sci.* **2005**, *60*, 2303–2316. [CrossRef]
255. Hartmann, H.; Derksen, J.J.; Van den Akker, H.E.A. Macroinstability uncovered in a Rushton turbine stirred tank by means of LES. *AIChE J.* **2004**, *50*, 2383–2393. [CrossRef]
256. Zhang, Y.H.; Yang, C.; Mao, Z.S. Large eddy simulation of the gas-liquid flow in a stirred tank. *AIChE J.* **2008**, *54*, 1963–1974. [CrossRef]
257. Li, Z.P.; Gao, Z.M.; Smith, J.M.; Thorpe, R.B. Large eddy simulation of flow fields in vessels stirred by dual Rushton impeller agitators. *J. Chem. Eng. Jpn.* **2007**, *40*, 684–691. [CrossRef]
258. Lu, Z.Y.; Liao, Y.; Qian, D.Y.; McLaughlin, J.B.; Derksen, J.J.; Kontomaris, K. Large eddy simulations of a stirred tank using the lattice Boltzmann method on a nonuniform grid. *J. Comput. Phys.* **2002**, *181*, 675–704. [CrossRef]
259. Feng, X.; Cheng, J.; Li, X.Y.; Yang, C.; Mao, Z.S. Numerical simulation of turbulent flow in a baffled stirred tank with an explicit algebraic stress model. *Chem. Eng. Sci.* **2012**, *69*, 30–44. [CrossRef]
260. Murthy, B.N.; Joshi, J.B. Assessment of standard k–ε, RSM and LES turbulence models in a baffled stirred vessel agitated by various impeller designs. *Chem. Eng. Sci.* **2008**, *63*, 5468–5495. [CrossRef]
261. Bałyga, J.; Kotowicz, M. Application of new chemical test reactions to study mass transfer from shrinking droplets and micromixing in the rotor-stator mixer. *Chem. Proc. Eng.* **2017**, *38*, 477–489. [CrossRef]
262. Singh, H.; Fletcher, D.F.; Nijdam, J.J. An assessment of different turbulence models for predicting flow in a baffled tank stirred with a Rushton turbine. *Chem. Eng. Sci.* **2011**, *66*, 5976–5988. [CrossRef]
263. Gimbun, J.; Rielly, C.D.; Nagy, Z.K.; Derksen, J.J. Detached eddy simulation on the turbulent flow in a stirred tank. *AIChE J.* **2012**, *58*, 3224–3241. [CrossRef]
264. Hartmann, H.; Derksen, J.J.; Montavon, C.; Pearson, J.; Hamill, I.S.; Van den Akker, H.E.A. Assessment of large eddy and RANS stirred tank simulations by means of LDA. *Chem. Eng. Sci.* **2004**, *59*, 2419–2432. [CrossRef]
265. Yeoh, S.L.; Papadakis, G.; Yianneskis, M. Numerical simulation of turbulent flow characteristics in a stirred vessel using the LES and RANS approaches with the sliding deforming mesh methodology. *Chem. Eng. Res. Des.* **2004**, *82*, 834–848. [CrossRef]
266. Yeoh, S.L.; Papadakis, G.; Lee, K.C.; Yianneskis, M. Large eddy simulation of turbulent flow in a Rushton impeller stirred reactor with sliding-deforming mesh methodology. *Chem. Eng. Technol.* **2004**, *27*, 257–263. [CrossRef]
267. Delafosse, A.; Line, A.; Morchain, J.; Guiraud, P. LES and URANS simulations of hydrodynamics in mixing tank: Comparison to PIV experiments. *Chem. Eng. Res. Des.* **2008**, *86*, 1322–1330. [CrossRef]
268. Laborde-Boutet, C.; Larachi, F.; Dromard, N.; Delsart, O.; Schweich, D. CFD simulation of bubble column flows: Investigations on turbulence models in RANS approach. *Chem. Eng. Sci.* **2009**, *64*, 4399–4413. [CrossRef]
269. Aubin, J.; Le Sauze, N.; Bertrand, J.; Fletcher, D.F.; Xuereb, C. PIV measurements of flow in an aerated tank stirred by a down- and an up- pumping axial flow impeller. *Exp. Therm. Fluid. Sci.* **2004**, *28*, 447–456. [CrossRef]
270. Montante, G.; Lee, K.C.; Brucato, A.; Yianneskis, M. Numerical simulations of the dependency of flow pattern on impeller clearance in stirred vessels. *Chem. Eng. Sci.* **2001**, *56*, 3751–3770. [CrossRef]
271. Ranade, V.V.; Tayalia, Y.; Krishnan, H. CFD predictions of flow near impeller blades in baffled stirred vessels: Assessment of computational snapshot approach. *Chem. Eng. Commun.* **2002**, *189*, 895–922. [CrossRef]
272. De La Concha, A.; Ramírez-Munoz, J.; Márquez-Baños, E.; Haro, C.; Alonso-Gómez, A.R. Effect of the rotating reference frame size for simulating a mixing straight-blade impeller in a baffled stirred tank. *Rev. Mexic. Ingen. Química* **2019**, *18*, 1143–1160. [CrossRef]

273. Wang, P.; Reviol, T.; Ren, H.; Böhle, M. Effects of turbulence modeling on the prediction of flow characteristics of mixing non-Newtonian fluids in a stirred vessel. *Chem. Eng. Res. Des.* **2019**, *147*, 259–277. [CrossRef]
274. Coroneo, M.; Montante, G.; Paglianti, A.; Magelli, F. CFD prediction of fluid flow and mixing in stirred tanks: Numerical issues about the RANS simulations. *Comp. Chem. Eng.* **2011**, *35*, 1959–1968. [CrossRef]
275. Maluta, F.; Paglianti, A.; Montante, G. RANS-based predictions of dense solid–liquid suspensions in turbulent stirred tanks. *Chem. Eng. Res. Des.* **2019**, *147*, 470–482. [CrossRef]
276. Antognoli, M.; Galletti, C.; Bacci di Capaci, R.; Pannocchia, G.; Scali, C. Numerical investigation of the mixing of highly viscous liquids with Cowles impellers. *Chem. Eng. Trans.* **2019**, *74*, 973–978. [CrossRef]
277. Guha, D.; Ramachandran, P.A.; Dudukovic, M.P.; Derksen, J.J. Evaluation of large eddy simulation and Euler–Euler CFD models for solids flow dynamics in a stirred tank reactor. *AIChEJ* **2008**, *54*, 766–778. [CrossRef]
278. Vakili, M.; Nars Esfahany, M. CFD analysis of turbulence in a baffled stirred tank—A three compartment model. *Chem. Eng. Sci.* **2009**, *64*, 351–362. [CrossRef]
279. Lane, G.L.; Schwarz, M.P.; Evans, G.M. Comparison of CFD methods for modeling of stirred tanks. In Proceedings of the 10th European Conference in Mixing, Delft, The Netherlands, 2–5 July 2000; pp. 273–280.
280. Beykal, B.; Boukouvala, F.; Floudas, C.A.; Sorek, N.; Zalavadia, H.; Gildin, E. Global optimization of grey-box computational systems using surrogate functions and application to highly constrained oil-field operations. *Comp. Chem. Eng.* **2018**, *114*, 99–110. [CrossRef]
281. Lane, G.L. Computational Modelling of Gas-Liquid Flow in Stirred Tanks. Ph.D. Thesis, University of Newcastle, Newcastle, New South Wales, Australia, 2006.
282. Kerdouss, F.; Bannari, A.; Proulx, P.; Bannari, R.; Skrga, M.; Labrecque, Y. Two-phase mass transfer coefficient prediction in stirred vessel with a CFD model. *Comput. Chem. Eng.* **2008**, *32*, 1943–1955. [CrossRef]
283. Torré, J.P.; Fletcher, D.F.; Lasuye, T.; Xuereb, C. An experimental and computational study of the vortex shape in a partially baffled agitated vessel. *Chem. Eng. Sci.* **2007**, *62*, 1915–1926. [CrossRef]
284. Montante, G.; Horn, D.; Paglianti, A. Gas–liquid flow and bubble size distribution in stirred tanks. *Chem. Eng. Sci.* **2008**, *63*, 2107–2118. [CrossRef]
285. Jaszczur, M. *Numerical Modeling of the Fluid-Particle Interactions in Non-Isothermal Turbulent Channel Flow with Dispersed Phase*; Publisher of AGH: Cracow, Poland, 2013.
286. Montante, G.; Paglianti, A.; Magelli, F. Experimental analysis and computational modelling of gas–liquid stirred vessels. *Chem. Eng. Res. Des.* **2007**, *85*, 647–653. [CrossRef]
287. Scargiali, F. Gas-Liquid Dispersions in Mechanically Agitated Contactors. Ph.D. Thesis, University of Palermo, Palermo, Italy, 2007.
288. Guan, X.; Li, X.; Yang, N.; Liu, M. CFD simulation of gas-liquid flow in stirred tanks: Effect of drag models. *Chem. Eng. J.* **2020**, *385*, 121554. [CrossRef]
289. Harvey, A.D.; Lee, C.K.; Rogers, S.E. Steady-state modeling and experimental measurement of a baffled impeller stirred tank. *AIChE J.* **1995**, *41*, 2177–2186. [CrossRef]
290. Ranade, V.V.; Van den Akker, H.E.A. A computational snapshot of gas-liquid flow in baffled stirred reactors. *Chem. Eng. Sci.* **1994**, *49*, 5175–5192. [CrossRef]
291. Brucato, A.; Ciofalo, M.; Grisafi, F.; Micale, G. Numerical prediction of flow fields in baffled stirred vessels: A comparison of alternative modelling approaches. *Chem. Eng. Sci.* **1998**, *53*, 3653–3684. [CrossRef]
292. Ranade, V.V. Computational fluid dynamics for reactor engineering. *Rev. Chem. Eng.* **1995**, *11*, 229–289. [CrossRef]
293. Ranade, V.V.; Dommeti, S.M.S. Computational snapshot of flow generated by axial impellers in baffled stirred vessels. *Trans. Inst. Chem. Eng.* **1996**, *74*, 476–484.
294. Luo, J.Y.; Gosman, A.D.; Issa, R.I.; Middleton, J.C.; Fitzgerald, M.K. Full flow field computation of mixing in baffled stirred vessels. *Chem. Eng. Res. Des.* **1993**, *71*, 342–344.
295. Murthy, J.Y.; Mathur, S.R.; Choudhury, C. CFD simulation of flow in stirred tanks reactor using a sliding mesh technique. In Proceedings of the 8th European Conference on Mixing, Cambridge, UK, 21–23 September 1994; pp. 155–162.
296. Dewan, A.; Buwa, V.; Durst, F. Performance optimizations of grids disc impellers for mixing of single phase flows in a stirred vessel. *Chem. Eng. Res. Des.* **2006**, *84*, 691–702. [CrossRef]
297. Luo, J.Y.; Gosman, A.D. Prediction of impeller-induced flow in mixing vessels using multiple frames of reference. As well as inner-outer method. *Inst. Chem. Eng. Symp. Ser.* **1994**, *136*, 549–556.

298. Brucato, A.; Ciofalo, M.; Grisafi, F.; Micale, G. Complete numerical simulation of flow fields in baffled stirred vessels: The inner-outer approach. *Inst. Chem. Eng. Symp. Ser.* **1994**, *136*, 155–162.
299. Naude, I.; Xuereb, C.; Bertrand, J. Direct prediction of the flows induced by a propeller in an agitated vessel using an unstructured mesh. *Can. J. Chem. Eng.* **1998**, *76*, 631–640. [CrossRef]
300. Lane, G.L.; Schwarz, M.P.; Evans, G.M. Chapter 34—Comparison of CFD Methods for Modelling of Stirred Tanks. In *10th European Conference on Mixing*; van den Akker, H.E.A., Derksen, J.J., Eds.; Elsevier Science: Amsterdam, The Netherlands, 2000.
301. Wechsler, K.; Breuer, M.; Durst, F. Steady and unsteady computations of turbulent flows induced by a 4/45 pitched-blade impeller. *J. Fluids Eng.* **1999**, *121*, 318–329. [CrossRef]
302. Glover, G.M.C.; Fitzpatrick, J.J. Modelling vortex formation in an unbaffled stirred tank reactors. *Chem. Eng. J.* **2007**, *127*, 11–22. [CrossRef]
303. Ammar, M.; Driss, Z.; Chtourou, W.; Abid, M.S. Effect of the tank design on the flow pattern generated with a pitched blade turbine. *Int. J. Mech. Eng. Appl.* **2012**, *2*, 12–19. [CrossRef]
304. Sossa-Echeverria, J.; Taghipour, F. Mixing of Newtonian and Non-Newtonian fluids in a cylindrical mixer equipped with a side-entry impeller. *Indust. Eng. Chem. Res.* **2012**, *51*, 15258–15267. [CrossRef]
305. Oshinowo, L.; Jaworski, Z.; Dyster, K.N.; Marshall, E.; Nienow, A.W. Predicting the tangential velocity field in stirred tanks using the Multiple Reference Frames (MRF) model with validation by LDA measurements. In *10th European Conference on Mixing*; van den Akker, H.E.A., Derksen, J.J., Eds.; Elsevier Science: Amsterdam, The Netherlands, 2000; Chapter 35; pp. 281–288.
306. Sommerfeld, M.; Decker, S. State of the art and future trends in CFD simulation of stirred vessel hydrodynamics. *Chem. Eng. Technol.* **2004**, *27*, 215–224. [CrossRef]
307. Patil, H.; Kumar, A.; Patel, K.A.; Harish, J.; Pant, J.H.; Vinod, V.A. CFD simulation model for mixing tank using multiple reference frame (MRF) impeller rotation. *ISH Eng.* **2018**, 1–10. [CrossRef]
308. Lee, K.C.; Yianneskis, M. The extent of periodicity of the flow in vessels stirred by Rushton impellers. *AIChE Symp. Ser.* **1994**, *9*, 5–18.
309. Zadravec, M.; Basic, S.; Hribersek, M. The influence of rotating domain size in a rotating frame of reference approach for simulation of rotating impeller in a mixing vessel. *J. Eng. Technol. Sci.* **2007**, *2*, 126–138.